The Paris Low-Level Jet During PANAME 2022 and its Impact on the Summertime Urban Heat Island

Jonnathan Céspedes[1,2], Simone Kotthaus[1], Jana Preissler[2,3], Clément Toupoint[2], Ludovic Thobois[2], Marc-Antoine Drouin[4], Jean-Charles Dupont[5], Aurélien Faucheux[6], and Martial Haeffelin[7]

[1]Laboratoire de Météorologie Dynamique (LMD-IPSL), CNRS, École Polytechnique, Institut Polytechnique de Paris, 91128 Palaiseau Cedex, France
[2]Vaisala France SAS, 6A rue René Razel, 91400 Saclay, France
[3]Dhara Consulting Services, Darmstadt, Germany
[4]LMD/IPSL, École Polytechnique, Institut Polytechnique de Paris, ENS, PSL Research University, Sorbonne Université, CNRS, Palaiseau France
[5]Institut Pierre Simon Laplace (IPSL), Université Versailles Saint-Quentin-en Yvelines, Palaiseau Cedex, France
[6]CEREA, École des Ponts ParisTech, EDF R&D, IPSL, Marne-la-Vallée, 77455, France
[7]Institut Pierre Simon Laplace (IPSL), CNRS, Palaiseau Cedex, France

Correspondence: Jonnathan Céspedes (jonnathan.cespedes@lmd.ipsl.fr)

Abstract.

Both the Low-Level Jet (LLJ) and the Urban Heat Island (UHI) are common nocturnal phenomena. While the canopy layer UHI has been studied extensively, interactions of the LLJ and the urban atmosphere in general (and the UHI in particular) have received less attention. In the framework of the PANAME initiative in the Paris region, continuous profiles of wind speed and vertical velocity were recorded with two Doppler Wind Lidars (DWL) - for the first time allowing for a detailed investigation of the summertime LLJ characteristics in the region. Jets are detected for 70% of the examined nights, often simultaneously at an urban and a suburban site highlighting the LLJ regional spatial extent. Emerging at around sunset, the mean LLJ duration is $\sim$10 h, the mean wind speed is $\sim$9 m s^{-1}, and the average core height is 400 m above the city. Many events show signatures in the temporal evolution that indicate that the inertial oscillation mechanism plays a role in the jet development: a clockwise veering of the wind direction and a rapid acceleration followed by a slower deceleration. The horizontal wind shear below the LLJ core induces variance in the vertical velocity (σ_w^2) above the urban canopy layer. It is shown that σ_w^2 is a powerful predictor for regional contrast in air temperature, as the UHI intensity decreases exponentially with increasing σ_w^2 and strong UHI values only occur when σ_w^2 is very weak. This study demonstrates how DWL observations in cities provide valuable insights into near-surface processes relevant to human and environmental health.

Copyright statement. TEXT

1 Introduction

The nocturnal Urban Heat Island (UHI) in the canopy layer is surely among the most studied phenomena in the urban environment. As this UHI is defined as the difference in air temperature between built-up and rural settings right above ground level (Oke et al., 2017), investigations usually focus on the near-surface atmosphere conditions, while the dynamics of the Atmospheric Boundary Layer (ABL) are rarely considered explicitly. Although wind speed and atmospheric stratification play a significant role in the formation of the UHI, the intensity of the UHI is strongest under low wind speed and cloud-free conditions (Oke et al., 2017), i.e., when atmospheric stratification in rural settings tends to be relatively stable. During stable atmospheric stratification, the atmospheric boundary layer flow may become decoupled from the friction exerted by the surface, which can lead to the formation of the nocturnal Low-Level Jet (LLJ). The LLJ is manifested by a sharp maximum in the vertical profile of the horizontal wind speed, typically at a height between $100\,\mathrm{m}$ and $1000\,\mathrm{m}$ above the ground, referred to as the core of the jet (Stull, 1988). Another feature related to the LLJ wind profile is a strong decrease that goes along with a minimum in the horizontal wind speed above the core height (Shapiro et al., 2016). The LLJ is a mesoscale phenomenon frequently observed in the ABL, mostly during nights with fair-weather conditions after clear-sky days. It is usually characterized based on its core height, wind speed and wind direction. With clear links to various processes such as advection, wind shear and turbulent mixing, the LLJ core characteristics can have a series of practical implications with respect to, e.g., air quality (Wei et al., 2023; Klein et al., 2019), changes in precipitation patterns (Algarra et al., 2019; Chen et al., 2022), aviation safety (Gultepe et al., 2019; Liu et al., 2014), the potential of, and risk to, wind energy production (Lundquist, 2021; Luiz and Fiedler, 2022; Rubio et al., 2022), urban ventilation (He et al., 2022), as well as the heat spatial distribution and intensity of the UHI effect (Kallistratova and Kouznetsov, 2012; Hu et al., 2013; Ulpiani, 2021; Lin et al., 2022). The LLJ is highly relevant for meteorology because its core characteristics are associated with the turbulent mass exchange in the ABL (Blackadar, 1957). Since the 1950s, the LLJ has been extensively documented, worldwide and throughout the year (Blackadar, 1957; Qi et al., 1999; Banta et al., 2002; Tuononen et al., 2017; Hartman, 2018; Du and Chen, 2019; Jiménez-Sánchez et al., 2019; Li and Du, 2021). One converging point of the previous studies is that the LLJ core generally is formed during the evening, followed by an increase in the core wind speed, and it eventually dissipates at about sunrise. Blackadar (1957) proposed the inertial oscillation theory to explain the physical mechanism behind the LLJ formation, but other mechanisms can also play a role. In The Great Plains, the LLJ formation is linked to the IO and the differential heating and cooling of the sloping terrain (Holton, 1967; Shapiro et al., 2016). Jets are also observed over coastal regions as the result of the land–sea breeze interactions and temperature gradients (Karipot et al., 2009; Roy et al., 2021). However, regardless of the study area or mechanism of formation, most of the observational-descriptive studies agreed on the importance of classifying the LLJ, usually by one of its main characteristics (Banta et al., 2002; Baas et al., 2009; Karipot et al., 2009; Bonin et al., 2015). Grouping of LLJ events into categories facilitates description and the analysis of potential effects on the environment of the affected area. The most widely used classification criterion is the core wind speed. Banta et al. (2002) were one of the first to propose four categories of wind speed to describe LLJs: (0-5), (5-10), (10-15) and (15-20) $\mathrm{m\,s^{-1}}$. Subsequently, several studies around the world have adopted similar categories of wind speed to study the LLJ (Karipot et al., 2009; Kallistratova et al., 2013; Wei et al., 2013; Arfeuille

et al., 2015; Vanderwende et al., 2015; Carroll et al., 2019). This classification system provides a better understanding of the LLJ phenomenon development, evolution, and impacts based on the wind speed intensity. Studies focused on the effects of the LLJ dynamics on the near-surface atmosphere, tend to consider other parameters like Turbulent Kinetic Energy (TKE), in addition to the core wind speed. Banta et al. (2002, 2003) successfully showed that the mechanical turbulence generated by the wind shear below the jet core plays a key role in controlling fluxes between the surface and the atmosphere. In particular, the downward transport of turbulence can modulate near-urban surface atmospheric processes like the UHI effect (Hu et al., 2013; Lin et al., 2022).

The UHI can be observed worldwide throughout the year, but in high-density cities in the mid-latitudes, it tends to be stronger during the summer (Lemonsu and Masson, 2002; Oke et al., 2017). The expansion of urban areas under poor ventilation and cooling design has made the UHI a prominent factor in the deterioration of the human thermal comfort (Kong et al., 2016; Li et al., 2019; Lin et al., 2022). High nocturnal temperatures increase the stress on the human body at times when it needs to rest (sleep), leading to higher mortality (Robine et al., 2008; Taylor et al., 2015; Ridder et al., 2016; He et al., 2022). While the UHI phenomenon is driven by excess heat in the built environment, atmospheric dynamics (advection, mixing, subsidence) significantly modulate the UHI intensity (Oke, 1973; Oke et al., 2017). Weak flow conditions favor the formation of strong UHI (Lemonsu and Masson, 2002), while each increase of $1\,\mathrm{m\,s^{-1}}$ in wind speed was found to reduce the urban air temperature during summer nights by up to $2\,^{\circ}\mathrm{C}$ (Cheng et al., 2012; He et al., 2022).

Although surface wind speed has long been recognized as an important indicator for variations in the UHI intensity, only a few studies in urban areas have investigated the relation between advection produced by the nocturnal LLJ and the UHI. Studies conducted in Sao Paulo, Brazil (Sánchez et al., 2022); Oklahoma, USA (Hu et al., 2013); Moscow, Russia (Kallistratova and Kouznetsov, 2012; Kallistratova et al., 2013); and Beijing, China (Lin et al., 2022); concluded that there is a negative correlation between the UHI intensity and the core wind speed of the jet. Even though these efforts have contributed to understanding the potential implications of the LLJ on UHI development, these works are mostly based on a limited number of radiosonde observations and few case studies. Hence, continuous observations of the wind speed profile with high temporal and spatial resolution are still needed in urban environments. Another relevant aspect of the interaction between the LLJ and the Urban Boundary Layer (UBL) is that the urban environment enhances atmospheric mixing and buoyancy that can again also affect the characteristics of those LLJs originated in the rural surroundings. In London, UK, Barlow et al. (2014) and Tsiringakis et al. (2022), have investigated the interaction between the LLJ and the UBL based on a combination of continuous DWL observations and modeling data, highlighting the importance of both the LLJ (downward mixing by shear-driven turbulence) and the urban surface (upward mixing driven by urban heat and roughness).

In France, the LLJ has been observed in northern coastal urban areas (Roy et al., 2021, 2022; Dieudonné et al., 2023), but coastal jets usually present different formation mechanisms and characteristics than those observed inland. This is mainly explained due to the importance of the sea-land breeze interactions (Karipot et al., 2009). Particularly in the urban area of Paris, some studies have been conducted to understand the impact of the LLJ on air quality, the mixing of pollutants within the UBL, and the UHI development. Klein et al. (2019) performed a one-day case study using a combination of DWL profiles, numerical simulations and ancillary observations, concluding that nocturnal LLJs can modulate the evolution of the mixing

layer with implications for the ozone concentration in the early morning. Cheliotis et al. (2021) collected DWL data during a period of 3 months in fall 2014, observing LLJs in 20 out of 63 nights. They linked the production of turbulent coherent structures to the presence of LLJ events, that in turn play an important role in the transport of heat, moisture and pollutants through the ABL. Wouters et al. (2013) presented a model-based case study during the Summer of 2006, where simulations of UHI and LLJ allowed them to conclude that the UHI could be affected by the nocturnal stability and mixing associated to the LLJ. However, when comparing with radiosonde profiles the strong jets were underestimated by the model, making it hard to identify what characteristics of the jets influenced the UHI development. Therefore, as far as the authors of the present work are aware, variations of the LLJ characteristics over periods exceeding a few days and their possible implications for UHI development have not yet been investigated in the Paris region. One key reason is the previous lack of medium or continuous long-term observations of the wind speed profile within the Paris UBL.

Strengthening the knowledge in this field is important because there is observational evidence that the LLJ is a common phenomenon in Europe, frequently detected at distances of less than $400\,\mathrm{km}$ from the city of Paris (Baas et al., 2009). Furthermore, gaining understanding about the LLJ impacts on the UHI is imperative, given the significance of UHI as a main concern in a city like Paris where a large number of inhabitants (approx. 12 million) is potentially exposed to severe heat hazards that are expected to become increasingly severe in future climates. As a consequence, the present study is going to investigate the characteristics and nocturnal temporal evolution of the LLJ observed over the Paris region in summer 2022, and what are their implications for the UHI intensity. For the first time, providing a comprehensive description of the occurrence of summertime LLJ in the Paris region and an analysis of its variability. Here, we assess the impact of the LLJ on the profile of the horizontal wind speed and the UHI intensity. This paper is structured as follows: Section 2 provides details of the study area, study period, DWL and surface-based meteorological observations, and automatic detection of LLJ and UHI determination; Section 3 presents the results of the LLJ detection and performance, LLJ classification, LLJ characteristics and wind profile, LLJ nocturnal evolution, and the UHI evolution; finally, Section 4 present the summary and conclusions of this paper.

2 Methods and materials

2.1 Study area and study period

Here we study the LLJ characteristics in the Paris region, France. With a population of over 12 million people, the Paris agglomeration is the second biggest megalopolis and the most densely populated city in Europe. The Paris region has experienced fast and wide urbanization during the last decades, but is still surrounded by natural and agricultural areas. Anthropogenic heat emissions and changes in land cover are aggravating the UHI effect (Lemonsu and Masson, 2002). Fig. 1 shows the topography of the Paris region, the land cover classification, and the geographical location of the experimental sites. Paris is located about $150\,\mathrm{km}$ from the sea, in a valley defined by the Seine River basin and surrounded by plateaus with modest topographic variation, which rise no more than $230\,\mathrm{m}$ above sea level (asl). In the city of Paris, the terrain is relatively flat, the lowest altitude is about $20\,\mathrm{m}$ asl along the river, and the highest is about $130\,\mathrm{m}$ asl on hills in the northern parts of the city. About $20\,\mathrm{km}$ southwest of the city, the Paris-Saclay Plateau is located, which has a mean extension of 10 km and is elevated about

160 m asl. It is an important economic, academic, and industrial area in the region. Due to the distance from the sea, there is no interaction of the sea breeze with the urban area. The long-term prevailing wind direction in the area is southwesterly and has a maritime origin, but winds from the northeast are also often observed (Haeffelin et al., 2005; Pal et al., 2012).
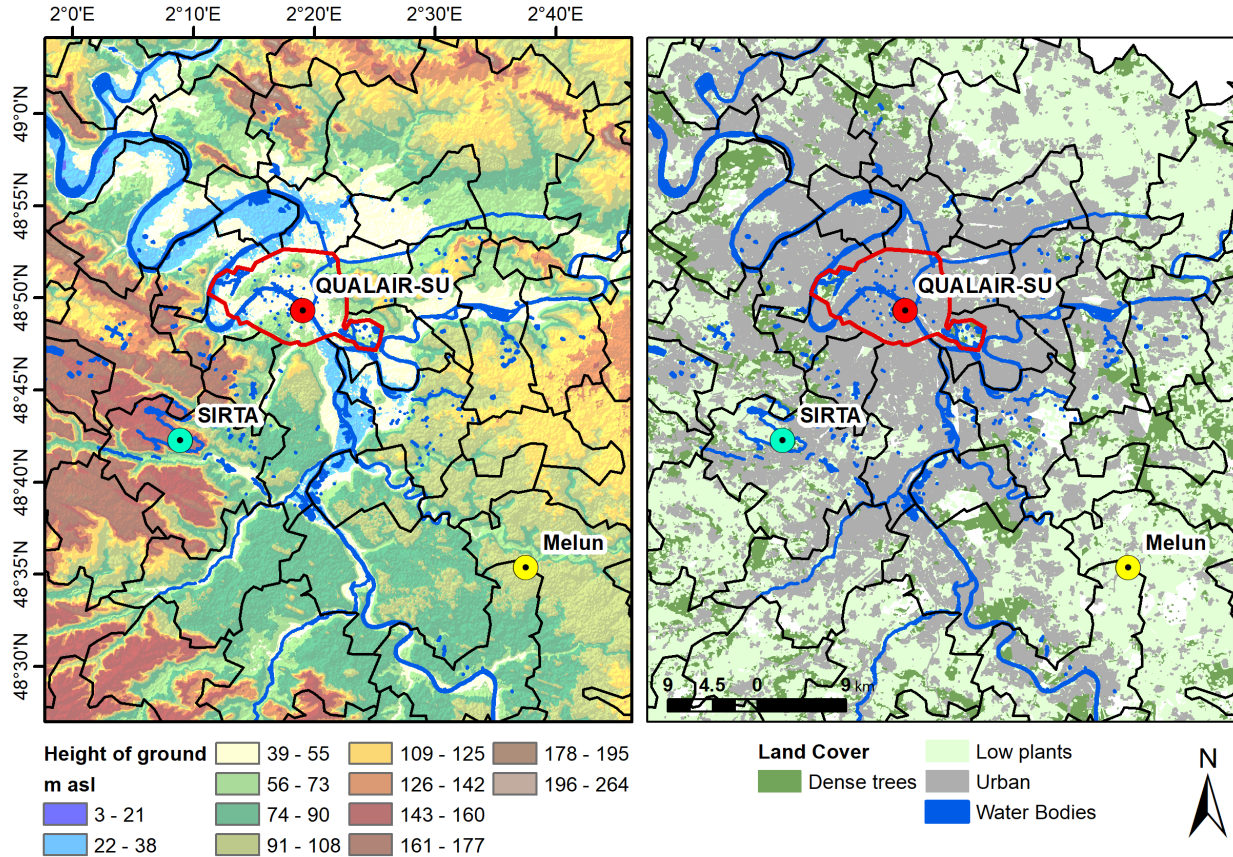
Figure 1. Paris region (France) study area and the location of the experimental sites. a) Topographic map from ESA (2023), and b) land cover map from Region (2023). The red borders indicate the administrative boundary of the City of Paris. The black polygons are administrative borders within the Paris region. The red dot represents the location of the WindCube Scan 400S at QUALAIR-SU (urban lidar), the cyan dot is the location of the WindCube WLS70 at SIRTA (suburban site), and the yellow dot is the location of Météo France meteorological measurement site at Melun (rural site).

This study focuses on the summer of 2022, between 15 June and 31 August. The year 2022 was recorded as the warmest observed in France so far, with three reported heat waves between June and August, leading to an exceptional nocturnal mesoscale flow over the Paris region during summertime with a predominant northeasterly flow. Severe conditions were observed especially in the July heat wave, where sea-level temperature anomalies above $12\,°C$ were associated with a deficit in precipitation rate of about 80%, leading to extreme droughts (Petit et al., 2023). In general, the summer of 2022 had prevailing winds com-

ing from the northerly to northeasterly directions (0°-75°), with speeds below $7\,\mathrm{m\,s^{-1}}$. The air temperature ranged between $11.8\,^{\circ}\mathrm{C}$ and $35.2\,^{\circ}\mathrm{C}$, with a mean value of $20.6\,^{\circ}\mathrm{C}$. These temperature values for 2022 are high when compared to longer-term averages. Using a comprehensive data set spanning from 2006 to 2022, collected by the Météo France surface meteorological network and processed by the ReOBS project (Chiriaco et al., 2018), the common of synoptic conditions within the study area are analyzed for the summer months of June, July, and August. The prevailing nocturnal winds exhibit a range of directions mostly between $170°$ and $45°$, with average speeds below $8\,\mathrm{m\,s^{-1}}$. The nocturnal air temperature ranges between $6.6\,^{\circ}\mathrm{C}$ to $38\,^{\circ}\mathrm{C}$, with a mean temperature of $18.6\,^{\circ}\mathrm{C}$.

2.2 Doppler Wind Lidar measurements

The Doppler Wind Lidar (DWL) measurements recorded during the study period (15 June and 31 August, 2022), both at the urban and the suburban sites contribute to the wind profile measurement network of the initiative PANAME (PAris region urbaN Atmospheric observations and models for Multidisciplinary rEsearch). The PANAME initieve is an unprecedented converge of multidisciplinary scietific investigations that promotes the synergy of numerous research projects that investigate the Paris urban environment in relation to weather, climate, air quality, and impacts on human health. The present study is part of the project so-called "DYNAMICS", which contributes to PANAME with an improved characterisation of nocturnal mean flow and turbulence conditions.

The high-power scanning DWL Vaisala WindCube Scan 400S was deployed in the city center of Paris (red dot in Fig. 1), on the roof of the Zamansky tower ($88\,\mathrm{m}$ above ground level (agl)) at the QUALAIR-SU supersite (48.8°N; 2.36°E; 125 m asl). QUALAIR-SU is a platform dedicated to atmospheric observations and air quality monitoring, which is operated by the Laboratoire Atmosphères, Observations Spatiales (LATMOS) and is hosted by Sorbonne Université, at the Jussieu campus (Qualair, 2022). The WindCube Scan 400S is a DWL equipped with a scanning head capable of orienting the laser beam in any direction of the hemisphere (Thobois et al., 2019; Dolfi-Bouteyre et al., 2008). The high energy emitted by the pulse, at $1.54\,\mathrm{\mu m}$ wavelength, allows it to sample the atmosphere at a distance of up to $7\,\mathrm{km}$. Several configurations of pulses are available corresponding to different spatial resolutions (75, 100, 150, or $200\,\mathrm{m}$) with a resolution of $75\,\mathrm{m}$ used in this study. A blind zone, spanning twice the spatial resolution ($150\,\mathrm{m}$ in this study), restricts measurements close to the sensor. Table 1 provides a summary of the main properties of the instrument. The WindCube Scan 400S can measure under different scanning strategies such as vertical stare, Plan-Position Indicator (PPI) and Doppler Beam Swinging (DBS). Liu et al. (2019) provide a detailed technical description of every scan mode operation and their potential applications. The DBS mode is widely used in urban meteorology to measure vertical profiles of horizontal wind speed and wind direction. It was shown by Pearson et al. (2009) that DBS operates fast and it well-capture unstable flows in the urban interface. In this study, a *five-point* DBS mode is used, with the scanning head successively addressing five lines of sight (LOS): one vertically oriented LOS (90° elevation angle) and four tilted LOS (75° elevation angle) pointing north, east, south, and west, respectively. Each scanning sequence (1 DBS cycle) is completed in approximately $15\,\mathrm{s}$, with $1\,\mathrm{s}$ of accumulation time for each LOS and $2\,\mathrm{s}$ between two LOS. The WindCube Scan 400S has been aligned with the geographic north, using the hard target method which has a precision of $\pm2°$.

Table 1. Properties of the Vaisala Doppler Wind Lidars WindCube Scan 400S (Urban site) and WLS70 (Suburban site). For the WindCube Scan 400s, the symbol (*) marks the setting used in this study.

Properties	WindCube Scan 400S (Urban)	WindCube WLS70 (Suburban)
Altitude Location (m asl)	125	155
Pulse repetition frequency (kHz)	7, 10*, 20, or 40	10
Pulse width (ns)	100*, 200, 400, or 800	100
Range gate resolution (m)	75*, 100, 150 or 200	50
Min range (m)	150	100
Max range (m)	7000	2000
Accumulation time (s)	1 per beam	1 per sequence
Radial wind speed range ($\mathrm{m\,s^{-1}}$)	± 30	± 30
Emission wavelength (μm)	1.54	1.54
Radial wind accuracy ($\mathrm{m\,s^{-1}}$)	0.1	0.3
Height location (m agl)	88	5
First available gate (m agl)	238	105

During the study period (15 June - 31 August 2022) the scan strategy was designed to follow an hourly schedule, integrating the DBS scan with the vertical stare and PPI. In the first half of every hour the DBS is performed for $9\,\mathrm{min}$, followed by a 3-minute full PPI at $0°$ of elevation with an angular resolution of $2°$/s, then $5\,\mathrm{min}$ of continuous vertical stare at $90°$ of elevation, followed by other $9\,\mathrm{min}$ of DBS and closing with other 3-minute full PPI at $0°$. The second half of hour repeats the same schedule. In this study, all vertical profiles of horizontal wind speed observations were derived from the DBS, while the vertical stare data are used to derive the Vertical Velocity Variance (σ_w^2). Observations from the PPI are not used in this study. The implemented scanning schedule was designed to fulfill several objectives but was not specifically optimized for the detection of LLJ. One quality control step is implemented to ensure a high-quality wind profile product, data with CNR (Carrier-Noise-Ratio) below $-20\,\mathrm{dB}$ and above $5\,\mathrm{dB}$ are excluded whereby omitting weak signals and clouds, respectively.

In addition to the observations in central Paris, data collected by a Vaisala WindCube WLS70 at a suburban location on the Plateau Saclay are used in this study. The data recorded with this instrument are used in this study only to highlight the regional scale of the LLJ observed. A detailed analysis of this data collection will be the subject of future studies. This profiling DWL is an instrument specially developed for meteorological applications (Cariou et al., 2009). The observations are conducted at the SIRTA observatory (Site Instrumental de Recherche par Télédetection Atmosphérique (Haeffelin et al., 2005)), located on the campus of Ecole Polytechnique in Palaiseau, $20\,\mathrm{km}$ southwest of Paris ($48.713°$N; $2.208°$E; $156\,\mathrm{m}$ asl; Fig. 1). Over the last 25 years, SIRTA has collected a comprehensive data set of atmospheric observations using in-situ measurements as well as passive and active remote sensing instruments, characterizing the regional atmospheric background of the Paris region (Dupont et al., 2016). The WindCube WLS70 uses a $1.54\,\mathrm{\mu m}$ pulsed fiber laser and a coherent detection system which provides

sufficient backscattering signal up to $4\,\mathrm{km}$. Every LOS performed by the WLS70 has a fixed spatial resolution of $50\,\mathrm{m}$ (see Table 1). The WLS70 performs four-point DBS measurements ($10\,\mathrm{s}$), in a similar way to the WindCube Scan 400S, but without the vertical LOS. This study uses 10-min averaged profiles, a previous quality control step is applied to these profiles to ensure a 80% of data availability at each range gate.

2.3 Automatic LLJ detection

Various methods and criteria have been developed to detect a LLJ in a vertical profile of horizontal wind, with techniques depending on the characteristics of the data source (e.g. limitations from measurement sensors) and even the study area. Stull (1988) defined a LLJ as any lower-tropospheric wind maximum in the vertical profile of horizontal wind speed, that is at least $2\,\mathrm{m\,s^{-1}}$ greater than speeds both above and below, within the lowest $1500\,\mathrm{m}$ of the atmosphere. This absolute criterion is widely found in the literature. It was applied to SODAR data collections (Karipot et al., 2009; Duarte et al., 2015) and radiosonde profiles measured in the USA (Bonner, 1968; Whiteman et al., 1997), and even in the Arctic Sea (Andreas et al., 2000). The threshold of this absolute criterion can be tuned as done by Banta et al. (2002), who used a value of $0.5\,\mathrm{m\,s^{-1}}$. However, under very weak flow conditions ($< 2\,\mathrm{m\,s^{-1}}$) the performance of the criterion could present limitations in the identification of LLJ events (Baas et al., 2009). In such cases, it is possible to use a relative threshold instead, in which a LLJ is detected by a velocity difference of 20%-25% between the local maxima and minima. In fact, absolute and relative thresholds have been combined to further improve detection. In different long-term radiosonde campaigns in Sao Paulo, Brazil, the criterion to identify a LLJ event in a single wind speed profile was that the maximum at the LLJ must be both greater than or equal to $2\,\mathrm{m\,s^{-1}}$ and 25% faster than the minimum above (Sánchez et al., 2022, 2020). Although in other DWL or SODAR-based studies, the same thresholds have been used, the high temporal and spatial resolution of surface-based remote sensing observations allows the incorporation of complementary steps. This enables not only an optimized detection of individual LLJ profiles but also the identification of LLJ events evolving over the time (Baas et al., 2009; Tuononen et al., 2015, 2017). In this study, the automatic LLJ detection is an adaptation from the method described by Tuononen et al. (2017) and uses 30-min averaged profiles of horizontal wind speed, to best combine the 15-min data products available at QUALAIR-SU and the 10-min data products available at SIRTA. This temporal resolution was previously used in SODAR studies presenting coherent LLJ detection (Karipot et al., 2009; Baas et al., 2009; Duarte et al., 2015).

Therefore, based on the literature and exploratory tests on the data set, some important conceptual aspects were adapted compared to the original method from Tuononen et al. (2017):

– Daytime LLJ events are negligible in the Paris region. During the day, very few LLJ events are recorded at the urban site. Therefore, this study focuses on the nocturnal periods, times between $18\,\mathrm{h}$ and $9\,\mathrm{h}$ UTC ($20\,\mathrm{h}$ and $11\,\mathrm{h}$ local time).

– The maximum height explored in every 30-min wind profile is $1000\,\mathrm{m}$ agl.

– In the study area, 99% of nocturnal periods present only one LLJ event within the ABL. Therefore, this study considers the presence of only one single LLJ event per night, unlike Tuononen et al. (2017) who accounted for the possible development of up to three simultaneous LLJ events within the ABL column in the same night.

210   Additionally, technical aspects of the algorithm were also adapted. In the following, a brief description of the implemented adaptations in this study is given, further details can be found in Tuononen et al. (2017):

- **LLJ detection from a single wind profile**: we consider every horizontal wind speed profile between the first available gate (238 m agl at QUALAIR-SU and 105 m agl at SIRTA) and 1000 m agl. A LLJ is identified in a profile if the local maximum of the horizontal wind speed is at least $1.5\,\mathrm{m\,s^{-1}}$ stronger than the first local minimum above or below. Note
215   that the minimum below the core height may not be captured correctly by the observations because no information is available $< 238\,\mathrm{m}$ agl in the instrument's blind zone. A relative detection criterion was tested, but it produced a high number of false negatives (43%).

- **LLJ event detection**: a LLJ event is considered as a coherent detection if lasts at least 2 h (i.e. four 30-min averaged profiles). However, an event is valid if at least three profiles are detected over the course of this period with the following
220   criteria for consecutive detections:

    - difference in core height $< 150\,\mathrm{m}$,
    - difference in core wind speed $< 20\%$,
    - difference in core wind direction $< 45°$,
    - difference in core time $< 1.5\,\mathrm{h}$.

225   The output parameters of the algorithm are listed as follows. i) LLJ occurrence: is a Boolean value (True [1] or False [0]) given to each profile; ii) LLJ core height: height of the maximum in the wind speed profile, in this case, the algorithm can provide it both in m agl and asl; iii) LLJ core speed: value of the wind speed at the core height; iv) LLJ core direction: wind direction at the height of the wind sped maximum. Additionally, the algorithm identifies the corresponding parameters for both the minimum above and below the jet core, in case they are recorded by the profile observations.

230   ## 2.4   Surface data and UHI determination

The UHI intensity ($\Delta\mathrm{UHI} = T_{urban} - T_{rural}$) is defined as the difference in air temperature between an urban (T_{urban}) and a rural (T_{rural}) site. Usually, standard meteorological observations at 2 m agl height are compared. In the current work, the QUALAIR-SU site (red dot in Fig. 1) is chosen as the urban site, and a Météo France station at Melun (48.613°N; 2.679°E; 91 m asl) is chosen as the rural site (yellow dot in Fig. 1).

235   Data collected at the QUALAIR-SU supersite were used to represent the central urban air temperature (T_{urban}) given that continuous and long-term observations are available. During the Intensive Observation Period (IOP) in the framework of PANAME-2022 campaign, surface-based meteorological stations were installed to capture the air temperature within the built environment at street level, e.g. at Place de la Madeleine (48.870 84°N; 2.324 32°N; 79 m asl) and Boulevard des Capucines (48.870 66°N; 2.331 75°N; 81 m asl) on 10 July 2022, i.e. later than the start of the analysis period of the current study (15
240   June 2022). Hence, data from the QUALAIR-SU meteorological station located at roof level (20 m agl) are here considered to

well represent the intensity of the ΔUHI for the Paris region. ΔUHI is stronger when using the street-level urban measurement sites by about $1\,°C$ when $ΔUHI > 6\,°C$ (see Fig. A1). Additionally, wind data collected from a $25\,m$ meteorological tower installed at Montsouris Park are used in this study to assess the relationship between ΔUHI and the near-surface wind speed.

The temperature at Melun is measured using a Sterela Opale UME at $2\,m$ agl, and that at QUALAIR-SU using a Vaisala WXT520 automatic weather station at $22\,m$ agl. The mean building height around the QUALAIR-SU site is about $25\,m$. 30-min averages are calculated for both sites to match the DWL analysis intervals. The average nocturnal UHI intensity is calculated as the mean of temperature differences recorded during the nocturnal period (sunset to sunrise). Additionally, based on cloud base height observations from a Lufft CHM15k automatic lidar ceilometer operated at the QUALIR-SU site, nights were classified into cloudy, partly cloudy, and cloud-free periods using the classification approach presented by Kotthaus and Grimmond (2018).

3 Results

3.1 LLJ detection performance

For the performance evaluation of the algorithm the time difference between two consecutive time steps for which a LLJ is detected gives an indication of the persistence of the jet event. The threshold sensitivity and performance analysis by Tuononen et al. (2017) revealed that the time-delta difference threshold has a strong influence on the performance of the algorithm. This may bias the algorithm towards the detection of false positives or very short events, which are not object of study in this work. The detection of false positives is further dependent on the quality of the measurements, which in turn depends on factors such as power and sensitivity of the laser system, vertical distribution of the aerosol load (tracers, see Section 2.2), and the presence of clouds.

An example of a coherent LLJ detection is presented in Fig. 2a. The jet core becomes visible in the late evening of the 9 August at 19h UTC at $550\,m$ agl, and with a wind speed of approximately $8\,m\,s^{-1}$. After sunset, the core height stabilizes at $500\,m$ agl and reaches a maximum wind speed between 21h and 23 UTC. After midnight, the core height increases beyond $550\,m$ agl, followed by a gradual decrease in the core wind speed. The jet persists throughout the night and into the early morning before it dissipates at 8h UTC on the 10 August. Fig. 2b presents a LLJ detection under weaker flow conditions and lower boundary layer height than the previous example. This LLJ event clearly failed the criterion of four consecutive detection explained in Section 2.2, and it is not considered in this study.

3.2 LLJ classification

By classifying LLJ according to their core wind speed magnitude, Banta et al. (2002) found that strong jets tend to occur at greater altitudes. Banta et al. (2003) studied the relationship between LLJ characteristics and turbulence within the stable nocturnal boundary layer, concluding that the core wind speed and core height can be used to diagnose turbulence effects in the region beneath the jet, considering that strong core wind speed are usually associated with strong turbulence below (Bonin
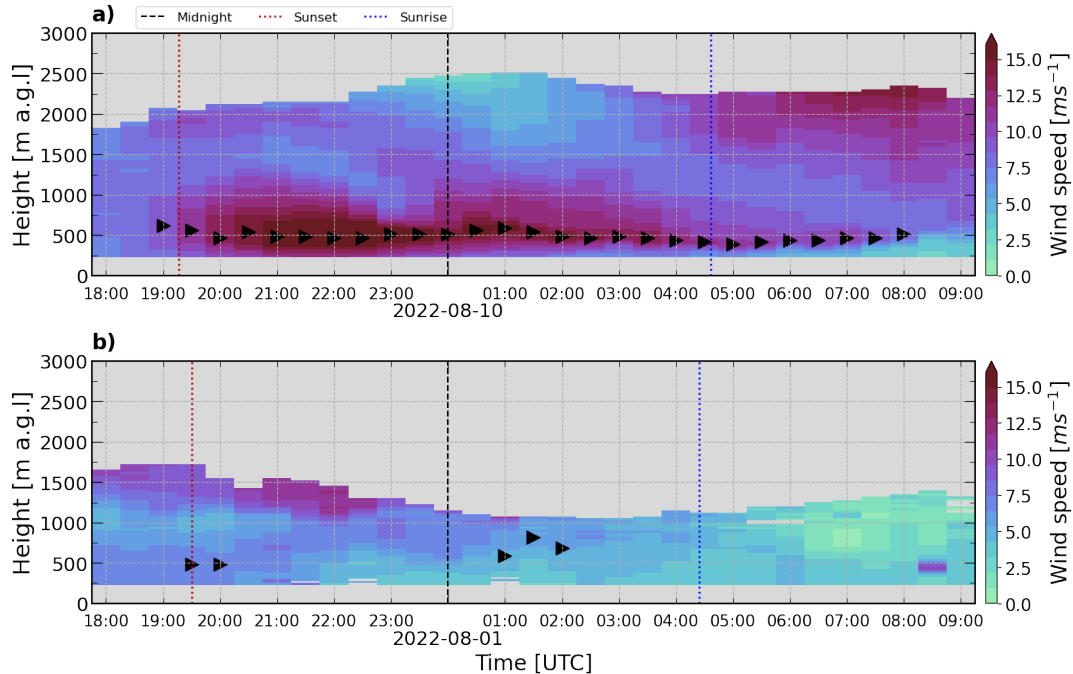
Figure 2. Time-height evolution of the horizontal wind speed. The temporal series are composited by 30-min average profiles retrieved by measurements performed by the WindCube Scan 400S at QUALAIR-SU (Urban site) between 18 - 09 UTC on a), between 9 and 10 August 2022, and b) 31 July to 1 August 2022. In both cases, the black triangles represent the core of the Low-Level Jet detected by the automatic procedure.

et al., 2015) and above the core (Conangla and Cuxart, 2006). In this study, both core wind speed and core height were tested as indicators for the classification of LLJ (not shown here), however, it was not possible to identify groups with consistent patterns in the LLJ characteristics. Hence, we found that the vertical velocity variance (σ_w^2) is a more meaningful indicator as it

275 effectively describes the link between the jet winds and surface-atmosphere exchanges. This turbulence quantity approximates the vertical component of the TKE during stable conditions (Banta et al., 2006). Here it is assumed that the σ_w^2 observations at the first range gate (238 m agl) of the DWL at the urban site is representative of the vertical mixing conditions in the nocturnal urban boundary layer. Each LLJ event is classified according to the mean nocturnal average σ_w^2 (between sunset and sunrise). Three classes are defined based on thresholds defined by the median and the 75th percentile of the distribution of σ_w^2 (Fig. 3):

280 indicating low ($< 0.11\,\mathrm{m^2s^{-2}}$), intermediate ($0.11\,\mathrm{m^2s^{-2}} \leq \sigma_w^2 < 0.23\,\mathrm{m^2s^{-2}}$), and high ($\geq 0.23\,\mathrm{m^2s^{-2}}$) vertical velocity variance, respectively.

3.3 LLJ characteristics

Based on the 79-day period spanning from 15 June 2022 to 31 August 2022, 55 nights (70%) exhibit a LLJ event at the urban QUALAIR-SU site. 96% (53 out of 55 nights) of these LLJ events were also detected over the suburban site at SIRTA, showing
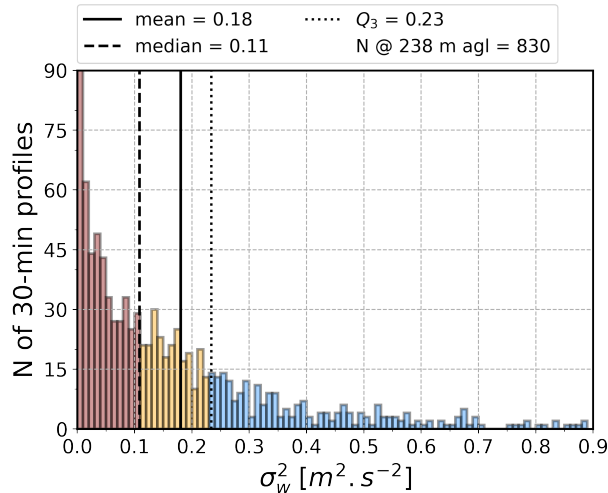
Figure 3. Histogram of the variance of the vertical velocity variance (σ_w^2) retrieved from vertical stare measurements at the first range gate at the urban site (238 m agl). The colors correspond to the σ_w^2 classes and are : low vertical mixing $\sigma_w^2 < 0.11\,\mathrm{m^2s^{-2}}$ (red), moderate vertical mixing $0.11\,\mathrm{m^2s^{-2}} \leq \sigma_w^2 < 0.23\,\mathrm{m^2s^{-2}}$ (orange), and strong vertical mixing $\sigma_w^2 \geq 0.23\,\mathrm{m^2s^{-2}}$ (blue). N = total number of 30-min profiles and Q_3 = Quartile 3, upper quartile.

285   that the nocturnal LLJ is a regional phenomenon in the Paris region. 6 out of 55 LLJ events were detected during cloudy conditions, but the complex interactions with cloud dynamics are beyond the scope of this work. Therefore, this study focuses on 49 nights (62% of the total of 79 nights in the study period) with a LLJ event detected at QUALAIR-SU under cloud-free conditions, in which 830 individual 30-min profiles (i.e. 415 h) were associated with a jet. According to these results, it is possible to say that the LLJ activity during summer Paris 2022 is high, specially when compared to previous studies conducted

290   in Paris during the autumn period or to other European studies of summertime LLJ activity. In the local context, Cheliotis et al. (2021) reported a 32% occurrence of LLJ during the fall of 2014 in Paris by using data collected by a DWL installed at QUALAIR-SU site. A climatological study at Cabauw, The Netherlands, found that LLJ occurred 32% of the time during summer, based on 7 years of SODAR profile data (Baas et al., 2009). At Utö, Finland, another climatological study reported an average occurrence of LLJ of 28% for the month of July, based on 2 years of DWL observations (Tuononen et al., 2017).

295   Outside Europe, a long-term study in Florida, USA, reported a 47% occurrence rate of LLJ during summer, based on 4 years of SODAR data (Karipot et al., 2009), and another work by Duarte et al. (2015) also reported a 47% occurrence rate in a summer study in South Carolina, USA.

     During the study period, the LLJ core height (Z_{LLJ}) ranges between 238 m agl and 950 m agl (Fig. 4a), i.e., throughout the entire height range considered for detection (Section 2.3). Note that for the 7% of 30-min profiles, when the core height

300   is detected at 238 m agl, the actual LLJ core may at times be located in the instrument blind-zone, i.e. below that level. Most jets (64%) have a core height between 300 and 500 m agl, with 350-400 m agl being the most common interval (22%). The median value of the LLJ core height is 388 m agl. These results are similar to previous case study analyses that found the

core height of LLJ in the Paris region at $400\,\mathrm{m}$ agl (Klein et al., 2019) and compare well with observations conducted over Greater London that reported core heights between 300 and $400\,\mathrm{m}$ agl (Tsiringakis et al., 2022). The analysis carried out at Boulogne-sur-Mer, France (about $200\,\mathrm{km}$ north of Paris) reports LLJ core heights $< 200\,\mathrm{m}$ (Roy et al., 2021). At this coastal site, it is likely that land-sea breezes play a role in the formation of the jet which might explain the occurrence of low-altitude core heights. At other European sites with coastal influence (Cabauw and Utö), lower Z_{LLJ} ($140\,\mathrm{m}$ agl) were observed during the summer (Baas et al., 2009; Tuononen et al., 2017).
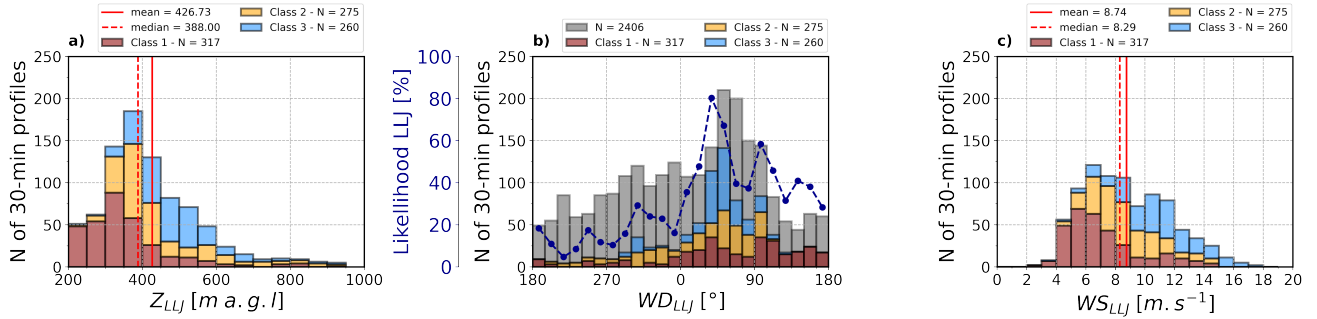
Figure 4. Histogram of a) the LLJ core height (Z_{LLJ}), b) the LLJ core wind direction (WD_{LLJ}), and c) the LLJ core wind speed (WS_{LLJ}). The colors of the bars represent the vertical mixing (σ_w^2) classes as defined in Fig. 3. In b) the gray bars denote the wind direction distribution at $400\,\mathrm{m}$ agl for all nocturnal periods between 15 June and 31 August 2022, and the dashed dark blue line represents the likelihood of a LLJ being detected from a given wind direction. In the legend class 1 (red), 2 (yellow) and 3 (blue) correspond to low, medium and strong vertical mixing classes, respectively.

The histogram of the LLJ core wind direction (WD_{LLJ}) (Fig. 4b), shows that LLJs are mostly observed under Easterly-Northeasterly flow during the study period in summer 2022. 66% of LLJs have a core wind direction between $0°$ and $105°$, with $30°$-$60°$ being the most common interval. LLJ profiles with northwesterly flow ($300° < WD_{LLJ} \leq 360°$) present an occurrence of 12%, while southeasterly flow ($105° < WD_{LLJ} \leq 180°$) contributes $\approx 14\%$ of the observed jets. The remaining 8% of the profiles are distributed in the interval $180°$ to $300°$. To assess how the LLJ over Paris relates to the general regional flow, the overall nocturnal wind direction distribution at $400\,\mathrm{m}$ agl (i.e. the level of the median Z_{LLJ}) is compared to the wind direction occurrence of LLJ events. The wind direction distribution of the LLJ follows a similar pattern as observed for the wind during the entire study period, where the northeasterly-easterly flow is predominant (44% of 2375 profiles). The likelihood of observing a LLJ is also higher in this sector with a 60% probability between $0°$ and $105°$, and the highest occurrence (80%) in the $30°$-$45°$ interval. Note that only two out of 49 jets (4%) present a southwest ($190°$-$300°$) wind direction, a sector that usually has a much larger frequency during summer nights with respect to the long-term climatology (2006-2022, Section 2.1).

Fig. 4c show that the LLJ core wind speed (WS_{LLJ}) varies between $2\,\mathrm{m\,s^{-1}}$ and $19\,\mathrm{m\,s^{-1}}$. For the majority of the jets (85%), the core wind speed ranges between $4\,\mathrm{m\,s^{-1}}$ and $12\,\mathrm{m\,s^{-1}}$, with a median value of $8.3\,\mathrm{m\,s^{-1}}$. This is again similar to the modeling results of the two-day case study in Paris reported by Klein et al. (2019), and comparable to a climatological study conducted in Jülich, Germany, a suburban area located $370\,\mathrm{km}$ from Paris in the northeasterly direction where the median

summer value of WS_{LLJ} is $8.3\,\mathrm{m\,s^{-1}}$ (Marke et al., 2018). Similarities are also found with Cabauw, The Netherlands (Baas et al., 2009), which is located in a suburban area $200\,\mathrm{km}$ from Paris in the northeasterly direction where the median value of WS_{LLJ} for summer is $\approx 9\,\mathrm{m\,s^{-1}}$. Given that both Cabauw and Jülich are located roughly upwind of Paris under Northeasterly flow, all these sites could be affected by the same LLJ event if the phenomenon has a large enough spatial extent as shown e.g. by Klein et al. (2019), which could explain these similarities in LLJ wind speed. However, the question of spatial extent goes beyond the scope of the current study. The median WS_{LLJ} found in this study is lower than the wind speeds reported for the summer in Utö, Finland, $11.6\,\mathrm{m\,s^{-1}}$ (Tuononen et al., 2017), and results from a study in Florida, USA $\approx 10\,\mathrm{m\,s^{-1}}$ (Karipot et al., 2009).

3.4 LLJ signature in the vertical wind profile

As introduced in Section 3.2, a σ_w^2-based classification system is used to identify LLJ events with common characteristics, and then study their potential impacts on the near-surface atmosphere. Fig. 4 shows that low σ_w^2 is mostly related to jets with a low core height between 238-350 m agl, which in turn present predominantly east-southeast wind direction (90°-180°), and low to intermediate core wind speed $< 7\,\mathrm{m\,s^{-1}}$. It should be noted, however, that LLJ events with core wind speed $> 10\,\mathrm{m\,s^{-1}}$ are also found in the low σ_w^2 class. These outliers are later discussed in Section 3.5. Jets with intermediate σ_w^2 occur mostly in two wind direction sectors: 300°-345° and 45°-105°. Their core height presents intermediate altitudes between 300 and 450 m agl, and wind speeds between 5-12 $\mathrm{m\,s^{-1}}$. In the strong σ_w^2 class, the core height tends to be $> 450\,\mathrm{m}$ agl, with a predominant northeasterly wind direction (30°-60°), and wind speeds $> 8.3\,\mathrm{m\,s^{-1}}$.

Fig. 5a presents the mean LLJ horizontal wind speed profile for each σ_w^2 class. Consistently with the histograms (see Fig. 4), the low σ_w^2 class present rather low values of wind speed throughout the profile. The core height of this profile is observed at $350\,\mathrm{m}$ agl and the wind speed at this altitude is $5\,\mathrm{m\,s^{-1}}$. The minimum wind speed above the core is $3.8\,\mathrm{m\,s^{-1}}$ and occurs at 1000 m agl, above this height the wind speed gradually increases. Similarly, the mean wind profile for the intermediate σ_w^2 class presents a core height at a slightly greater altitude of $400\,\mathrm{m}$ agl, but with a slightly higher wind speed, about $6.2\,\mathrm{m\,s^{-1}}$. The minimum above the core is close to that of the low-variance class. The mean profile associated with the strong σ_w^2 class exhibits a distinctly different shape and stronger wind speeds. The core height is located at $475\,\mathrm{m}$ agl, i.e. $75\,\mathrm{m}$ higher than the moderate σ_w^2 profile. The core wind speed is about $9.2\,\mathrm{m\,s^{-1}}$, which is 50% and 30% stronger than the core wind speed for the low and intermediate σ_w^2 class, respectively. The minimum above the core is about $3.8\,\mathrm{m\,s^{-1}}$ and located at 1750 m agl, i.e. at greater altitudes than for the other two classes.

The respective median profiles of σ_w^2 for each class are presented in Fig. 5b, which illustrate that LLJ core height not only influences the horizontal wind speed but also the vertical mixing. For all three median profiles, the strongest vertical mixing is retrieved from data recorded at the first range gate of the lidar ($238\,\mathrm{m}$ agl), i.e. closer to ground level. Above this height, the median σ_w^2 values gradually decrease, reaching values close to zero, above the respective jet core shown in Fig. 5a. As the minimum recorded altitude of the vertical stare depends on the blind zone of the DWL, no information on the vertical velocity variance below $238\,\mathrm{m}$ agl is available. In general, the shape of the three median profiles agrees with those reported in previous
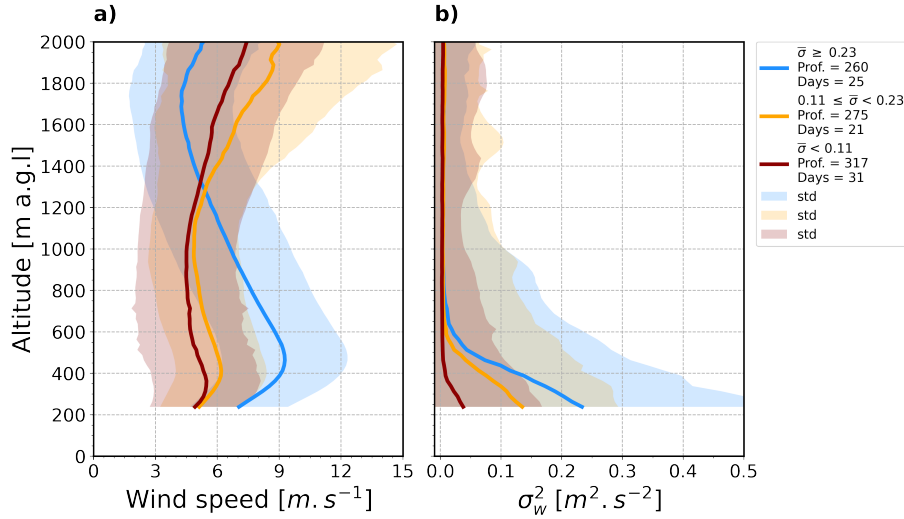
Figure 5. Mean profiles of a) horizontal wind speed and b) median profiles of vertical velocity variance σ_w^2. The solid lines represent the composite profile with all 30-min profiles detected as LLJ, and the shadows denote 1±SD. Each panel presents the respective profiles for each σ_w^2 class: red is low σ_w^2, orange is moderate and blue is strong σ_w^2.

studies (Banta et al., 2006; Bonin et al., 2015). In cities, unstable or neutral stratification and higher σ_w^2 are mantained by the added urban heat (Theeuwes et al., 2019).

To conclude, the classification system used here in this study allows us to identify the following trends: i) in the low σ_w^2 class the LLJ profiles are detected in a wind direction sector between $0°$ and $180°$. This class represents all the profiles detected in the southeast sector between $105°$ and $180°$, all the low altitude cases in the interval between 250 and $300\,\mathrm{m}$ agl, and is the dominant class for profiles with a core wind speed $< 6\,\mathrm{m\,s^{-1}}$. ii) The intermediate σ_w^2 class is detected in a wide wind direction sector between $300°$-$115°$, and dominates the northwest sector between $300°$-$360°$. The values of core height range between 300-450 m agl, while the core wind speed varies between 5-12 $\mathrm{m\,s^{-1}}$. iii) Finally, profiles in the strong σ_w^2 class occur in the wind direction sector between $0°$-$115°$, but are usually found at the northeast sector between $30°$ and $60°$. LLJs in this category can present core height at high altitudes $> 400\,\mathrm{m}$ agl with a strong core wind speed $> 8.3\,\mathrm{m\,s^{-1}}$.

3.5 LLJ nocturnal evolution

According to Stull (1988), a LLJ typically forms during the night and reaches its maximum wind speed before dawn hours, between midnight and 4h local time. Fig. 6a presents an example of a well-defined nocturnal LLJ event observed in Paris during the night between the 16-17 July 2022, showing both the characteristics of the LLJ core and the minimum above. The WS_{LLJ} is about $7.5\,\mathrm{m\,s^{-1}}$ before sunset, then it increases and reaches its maximum ($12.5\,\mathrm{m\,s^{-1}}$) at 2.5 h after sunset (22h30 UTC and 00h30 LT), then starts to decrease again up from about 1 h before sunrise. The Z_{LLJ} is about $750\,\mathrm{m}$ agl at sunset when the convective boundary layer is still collapsing. When WS_{LLJ} starts to increase after sunset (21h UTC), Z_{LLJ} decreases to

around $400\,\mathrm{m}$ agl and remains around this altitude throughout the night. At sunset, the jet core follows a northeasterly flow that veers toward the east over the course of the night by $90°$. The lack of sudden changes indicates that there are no changes in air mass.
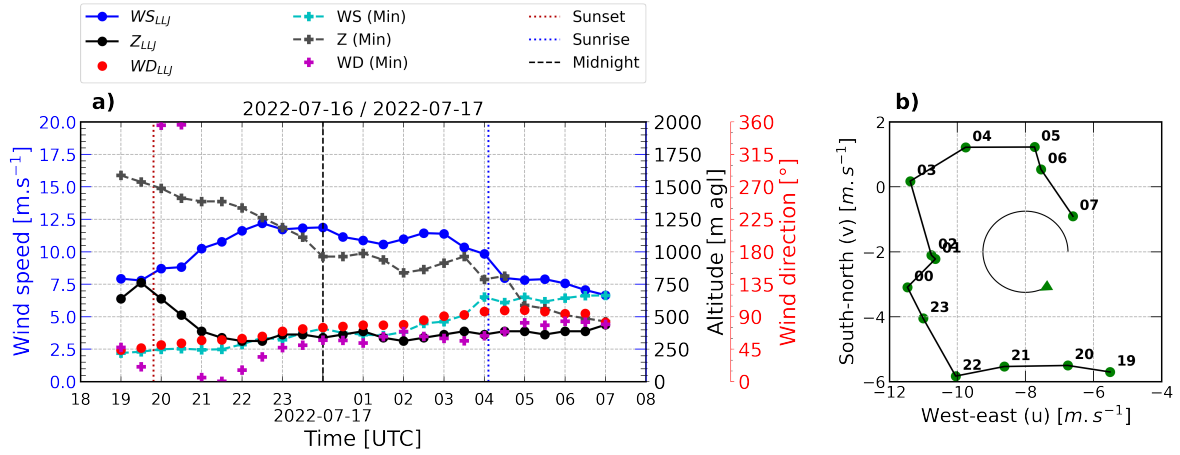
Figure 6. Nocturnal evolution of an individual LLJ event (16-17 July 2022) with a) illustrating the jet characteristics: core wind speed (WS_{LLJ}) and the minimum above (WS_{Min}), core height (Z_{LLJ}) and the height of the minimum above (Z_{Min}), core wind direction (WD_{LLJ}) and wind direction of the minimum above (WD_{Min}); and b) the wind hodograph based on the meridional and zonal components of the wind (u, v) at the height of the core of the jet. The green arrow indicates the sense in which the wind is veering during the night (clockwise). Labels indicate the hour from 19h of 16 July to 07h of 17 July (UTC).

The development of the wind speed minimum above the LLJ core (see Fig. 5a) and the evolution of its characteristics are in accordance with the momentum budget of the atmospheric column in the ABL during a LLJ event (Blackadar, 1957). The wind speed is weak ($\approx 2.5\,\mathrm{m\,s^{-1}}$) at sunset and then experiences a slight increase over the course of the night. The height of this minimum is located about $900\,\mathrm{m}$ above the LLJ core at sunset and then gradually decreases until it merges with the jet core at the time of the jet dissipation. The wind direction of the jet core and the minimum above differ by about $50°$ at sunset and then slowly converge over the course of the night before converging again at about $1\,\mathrm{h}$ past sunrise. Overall, the wind speed, wind direction and height in the jet core and the minimum above show distinct contrasts during the time of jet formation and then reach a common point at 7h UTC when the jet is completely dissipated and the momentum is distributed evenly over the entire column in the ABL.

This LLJ evolution (Fig. 6) suggests that the Inertial Oscillation (IO) is the formation mechanism of this event (Blackadar, 1957; van de Wiel et al., 2010). 28 out of 49 (57%) of the cloud-free detections reported in this study present a similar nocturnal evolution, which suggests that the IO is highly relevant for the jet dynamics in the Paris region. The IO is characterized by an oscillation of the wind above the elevated nocturnal temperature inversion with a period of $T = 2\pi/f$, where f is the Coriolis parameter ($f = 2\Omega\sin\theta$, with Ω and θ being the angular speed of the Earth's rotation and latitude, respectively). At the QUALAIR-SU latitude ($\theta \approx 48.84$), this gives $T \approx 16\,\mathrm{h}$, which is approximately the duration of the most persistent LLJ

events observed here, e.g. 7-10 August (see Fig. 8). The amplitude of this wind speed oscillation is related to the magnitude of the ageostrophic velocity component, and can cause the core wind speed to reach supergeostrophic magnitude. In addition to a gradual increase and decrease (*wind speed oscillation* hereafter) of the core wind speed, the IO is associated with a clockwise change in wind direction, which is clearly evident from the time series (Fig. 6a) and also illustrated by the hodograph of the meridional and zonal wind components (u, v) (Fig. 6b).

Fig. 7 presents the nocturnal evolution of the core wind speed for the 49 jets observed under cloud-free conditions during the study period, classified into three groups of σ_w^2 intensity (section 3.2). In the low σ_w^2 class, 15 out of 19 (79%) cases do not show the wind speed oscillation, as opposed to four visible outliers (16 and 19 July, and 11 and 13 August). These outliers do not show common behavior in terms of duration, acceleration or peak wind speed. These cases are associated with a strong stable atmospheric stratification caused by the advection of hot air masses (Kotthaus et al., 2023), but these details are beyond the scope of this study and will be investigated elsewhere. Omitting those outliers, the behavior of the median wind speed curve for the low σ_w^2 class is rather flat with a mean value of $6.23 \, \mathrm{m\,s^{-1}}$. For the events with moderate σ_w^2 values (Fig. 7b), the median wind speed curve is stronger, with a mean value of $8.07 \, \mathrm{m\,s^{-1}}$. It increases slightly, starting from $2 \, \mathrm{h}$ after sunset and reaches its maximum at about 4-5 h later, before starting to slowly decay until dissipation. Finally, for the strong σ_w^2 class (Fig. 7c) most of the events exhibit a clear wind speed oscillation in wind speed. The acceleration starts with the jet formation and lasts until $3 \, \mathrm{h}$ after sunset. A peak in the core wind speed is observed at around midnight ($\pm 2 \, \mathrm{h}$), followed by a slow deceleration until dawn hours with a mean value of $10.2 \, \mathrm{m\,s^{-1}}$. The median WS_{LLJ} is $9 \, \mathrm{m\,s^{-1}}$ at $1 \, \mathrm{h}$ before sunset (i.e., in the order of magnitude as the peak of the wind speed median in the moderate σ_w^2 class) and then a gradual increase is produced until it reaches the maximum peak at $2 \, \mathrm{h}$ after sunset, which lasts about $2 \, \mathrm{h}$. The WS_{LLJ} gradually starts to decay from about $4 \, \mathrm{h}$ after sunset until it reaches a minimum right before sunrise, which is associated with the jet dissipation given.
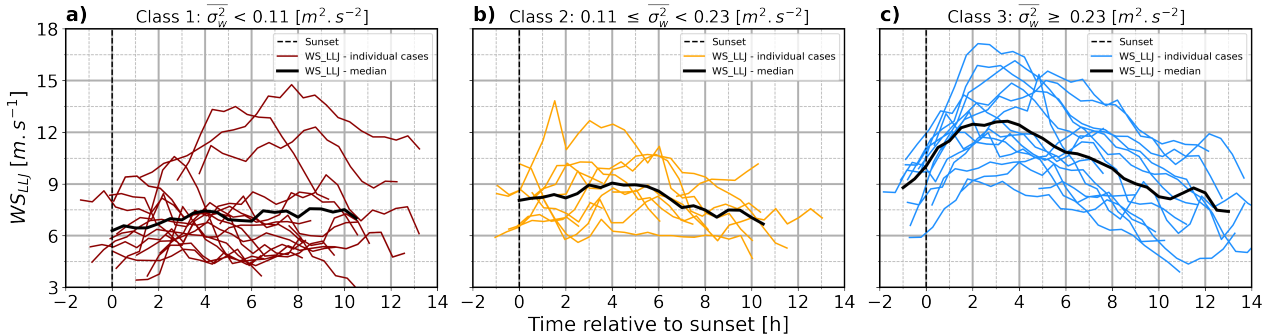
Figure 7. The evolution of the core wind speed throughout the night for each LLJ event classified by a) low, b) intermediate, and c) strong vertical mixing. The black line represents the median for each group, which is calculated for times with a minimum of three samples.

3.6 Temporal distribution of the LLJ characteristics

Fig. 8 presents the time series of the nocturnal evolution for the three jet core characteristics (height, wind speed and wind direction) for each event during the study period, including the cloudy nights. An amplitude in wind speed can clearly be identified for 25 out of 49 (i.e. 51%) jets, mainly observed for jets with strong vertical velocity variance (as shown in Fig. 7c) and high core height. This trend is also valid for short-duration cases ($< 4\,\mathrm{h}$), for example, 16 July. Nocturnal evolution of the core direction (Fig. 8b) shows that 28 out of 49 (i.e. 57%) of jets present a persistent clockwise veering with an average change in wind direction of $3.7\,^\circ\mathrm{h}^{-1}$. Two cases particularly stand out with a strong veering ($> 5\,^\circ\mathrm{h}^{-1}$): 28 June and 21 August. They fall into the intermediate and low σ_w^2 class, respectively, and both emerge from a northwesterly direction (322° and 282°, respective initial core direction). As discussed (Section 3.5), both the wind speed oscillation and the clockwise veering are signatures of the IO formation mechanism. However, not all cases with wind speed oscillation (Fig. 6a) present necessarily a strong clockwise veering (Fig. 6b). For example, jets detected between the 7 and 9 of August show the wind speed oscillation, but their change in core wind direction is less than $1\,^\circ\mathrm{h}^{-1}$, remaining almost constant in wind direction.

These time series showcase in detail the variability in the LLJ duration as well as the timing of both formation and dissipating. Results show that 29 out of 49 (i.e. 59%) jets last almost the entire night, emerging at sunset $\pm 2\,\mathrm{h}$ and dissipating at sunrise $\pm 2\,\mathrm{h}$. However, jets can emerge in the middle of the night and continue even after sunrise. 31 out of 49 (i.e. 61%) cases last more than $8\,\mathrm{h}$, including cases with late starting time (up to $4\,\mathrm{h}$ after sunset). During the study period, the maximum LLJ duration is $15\,\mathrm{h}$, the minimum duration is $2\,\mathrm{h}$ (by conceptual definition), and the mean duration is $9.5\,\mathrm{h}$.

The day-to-day variability highlighted in Fig. 8a reveals the influence of synoptic conditions for the LLJ characteristics. While some cases appear to be isolated (e.g. 28 June and, 10 July), during consecutive LLJ detection the characteristics of their core may vary night after night or may be similar each night. Ten events are detected between 10-19 July (heatwave period) with strong day-to-day variability in terms of σ_w^2 levels and the core characteristics. During this period, jets at high core height and strong wind speeds are associated with strong σ_w^2, while slow and low-altitude jets present weak σ_w^2. A different situation is observed for the seven jets detected between the 06-13 August. Persistent synoptic conditions are prevail for the first five detections between 06-10 August, with similar nocturnal evolution of core characteristics and vertical mixing. However, the last two detections on the 11 and 13 August (outliers in Fig. 7) differ clearly from this period as they have short duration, low core height, weaker wind speed, and low vertical mixing.

The persistence of synoptic conditions results in a certain clustering of the LLJ events. For example between 15 and 18 June, four consecutive events present similar duration (10-12 h), with similar speeds (6-$9\,\mathrm{m\,s}^{-1}$), and similar core heights at altitudes ($< 400\,\mathrm{m}$ agl). In the period between 6 and 10 August, the detected events present similar core characteristics with strong wind speed oscillation at high altitudes, occurring in the northeast flow with a wind direction veering becoming more pronounced from one night to the next. These cases present very similar nocturnal evolution and duration, and all of them fall into the same σ_w^2 class (strong vertical mixing). In the period between 3 and 6 July again, after four consecutive days with no detection, four short events ($< 5\,\mathrm{h}$) are found at medium to high altitudes between 400 and $600\,\mathrm{m}$ agl, with wind speeds between 10 and $12\,\mathrm{m\,s}^{-1}$.
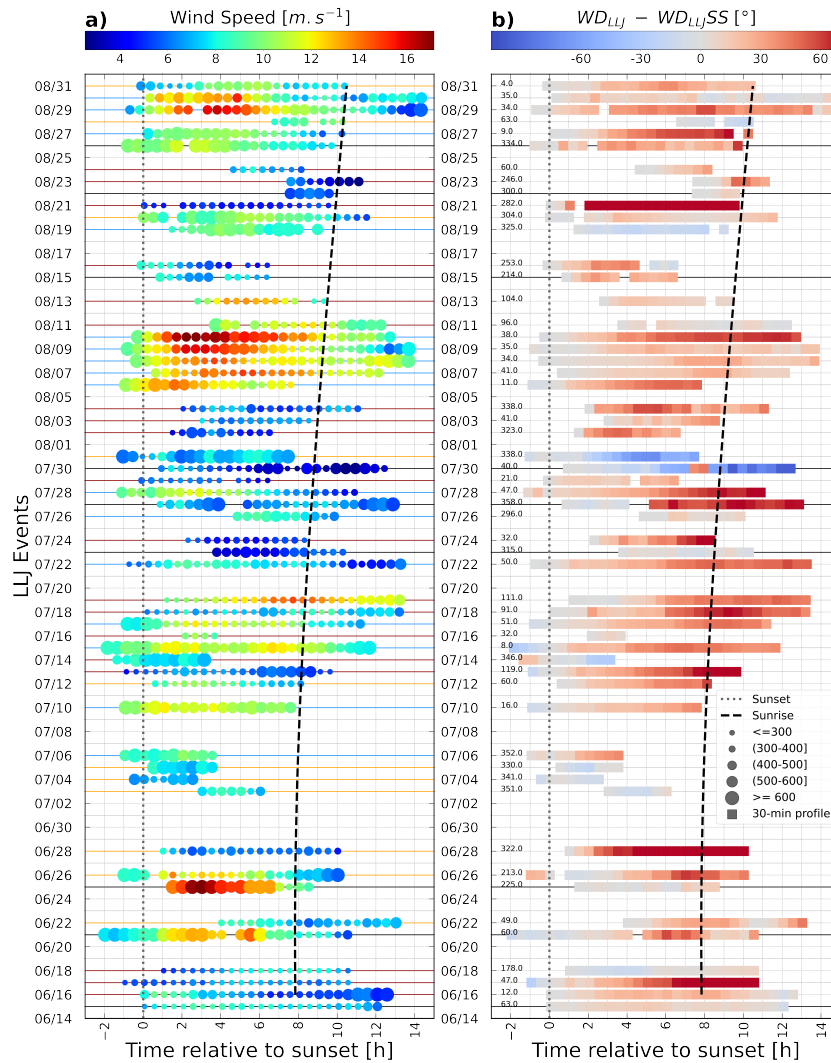
Figure 8. Nocturnal evolution of the LLJ events during the study period 15 June - 31 August 2022 at 30 min resolution in time relative to sunset (dotted line). In a) dot size and color indicate the jet core altitude (Z_{LLJ}) and wind speed (WS_{LLJ}), respectively. Horizontal lines represent the vertical mixing category of each case: low (red), intermediate (orange), and strong vertical mixing (blue). b) Core wind direction (WD_{LLJ}) variability relative to the wind direction at sunset ($WD_{LLJ}SS$) or initial wind direction when the jet is formed in the middle of the night (indicated with the number inside the plot frame, at the left side). Horizontal black lines mark dates that are excluded from further analysis due to cloud conditions in a) and b). The dashed line marks the time of sunrise.

As discussed in Section 3.3, LLJ in a narrow easterly sector (80°-115°) are all associated with low vertical velocity variance. Fig. 8 reveals that these specific LLJ events (18 and 19 July, and 11 and 13 August) in fact present the high wind speed outliers detected in Section 3.5 with a distinct wind-speed amplitude (Figure 7a) and clockwise veering (Fig. 8b). It is further evident that these easterly jets are found at relatively low altitudes ($< 350\,\mathrm{m\,agl}$) suggesting a channeling along the low topography

450 of the river Marne basin towards the East of Paris could play a role in the acceleration mechanisms. These processes will be investigated in future studies.

3.7 LLJ impacts on UHI

Cloudiness and wind are environmental variables that exert an essential control on the intensity of the UHI and its nocturnal evolution. The UHI of the canopy layer is generally strongest during cloud-free nights and low wind speed conditions, following

455 days with the same characteristics (Oke et al., 2017). Fig 9a presents the relationship between the nocturnal mean surface wind speed at the urban park Montsouris and the nocturnal mean ΔUHI intensity in the Paris region, including only cloud-free nights after fair-weather days to focus the analysis on wind effects only. Wind data at Montsouris park are observed at a tower $25\,\mathrm{m}$ agl, a measurement setting not often available in urban areas. The UHI intensity decreases exponentially with increasing wind speed. Based on observations from different cities in Canada, Oke (1973) proposed an empirical formulation where the

460 mean ΔUHI is inversely proportional to the square root of the average regional nocturnal surface wind speed ($\Delta UHI \propto \overline{ws}^{-\kappa}$, κ being a dimensionless parameter often equal to 0.5). The urban wind direction at Montsouris suggests that weak values of ΔUHI are mostly found under northeasterly flow. This wind direction sector is characterized by LLJ with strong wind speeds and high σ_w^2 values. A best fit to the Paris data following this relation is included in Fig. 9a and describes a function that follows the drop in ΔUHI due to the increase in wind speed, with an asymptotic shape defined by the threshold ΔUHI $\sim 1\,^\circ\mathrm{C}$, which

465 appears to be the baseline ΔUHI intenisty for summertime cloud-free conditions.
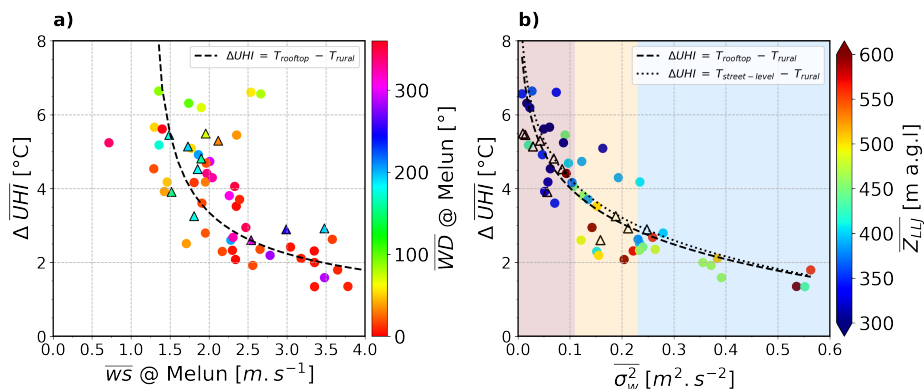
Figure 9. Relations between nocturnal average of ΔUHI intensity for all cloud-free nights in the study period and a) $10\,\mathrm{m}$ agl wind speed at Montsouris park, an urban reference site. The dots are colored by surface wind direction at Montsouris. The dashed black curve is the best fit to the data: $y = 4((x - 1.1)^{-0.8})$, and it follows the empirical relationship described by Oke (1973) b) the vertical velocity variance (σ_w^2) at $238\,\mathrm{m}$ agl, dots are colored by the LLJ core height above the ground surface. The dashed black curve represent the best non-linear fit found for the data collected in the Paris region, and determining ΔUHI intensity with QUALAIR-SU data. The dotted black curve represents the same but using data collected by a surface-based station installed at Boulevard de Capucines for a shorter time period (see Section 2.4). Both curves represent the equation: $y = -1.39\log(x) + 0.84$. The background shading indicates the LLJ classes described in Section 3.2. In all subplots, dots and triangles represent nights with and without LLJ events, respectively.

The near-surface urban wind speed, sampled at a height (25 m agl) slightly above the mean building height of 20 m, provides insights on advection processes. However, to assess the role of vertical mixing on spatial contrasts in air temperature, the response of ΔUHI to the vertical velocity variance at 238 m agl is shown in Fig 9b. This relation is even more clearly pronounced as can be seen from the smaller error statistics listed in Table 2. Given wind observations above the urban canopy layer (as here at Montsouris Park) are rarely available, the wind speed observations at the rural site Melun were also tested to have a full view of the ΔUHI response to the regional winds. As the rural near-surface wind speeds are associated with a higher uncertainty when predicting the ΔUHI, it is concluded that turbulence observations inside the urban boundary layer show a closer link to the processes that drive the UHI development. The curves in Fig 9b represents the best non-linear model fitted to the data collected during the nights with a LLJ event, using the T_{air} data collected at QUALAIR-SU. We also add the fit resulting from the data collected by the IOP station at Boulevard des Capucines (see Section 2.4). The similarity between the two curves shows that the relationship between ΔUHI and σ_w^2 is preserved even when using QUALAIR-SU data collected at roof-level.

Table 2. Error metrics for prediction of ΔUHI prediction. In order of appearance from left to right: following the surface wind speed relationship proposed by Oke (1973), the best-fit model to urban and rural surface wind speed at Melun site and vertical velocity variance (σ_w^2) in the urban boundary layer above the roughness sublayer, respectively. The metrics are Mean Square Error (MSE), Root Mean Square Error (RMSE), Mean Absolute Error (MAE), and determination coefficient (R^2).

ΔUHI Estimator parameter	urban surface wind	rural surface wind	σ_w^2
MSE	2.18	2.89	0.65
RMSE	1.48	1.70	0.81
MAE	1.23	1.19	0.63
R^2	-0.18	-0.21	0.70

These results are consistent with findings by Bonin et al. (2015) and Banta et al. (2006), who showed that the mixing below the LLJ core can affect the turbulent exchange processes near the surface. Table 3 presents a summary of the average values of ΔUHI and the LLJ characteristics, corresponding to each σ_w^2 class. Weak vertical mixing is associated with strong ΔUHI, calm winds and shallow core heights, whereas strong mixing relates to weak ΔUHI and strong wind speeds and greater core heights. Previous studies have shown that jets at low altitudes (up to 300 m agl) tend to present low to moderate core wind speeds (Banta et al., 2002; Karipot et al., 2009; Carroll et al., 2019), so that weak wind shear only produces little mechanical turbulence. These low-altitude jets are often associated with a strong temperature inversion over the rural surfaces, so that the stable stratification of the atmosphere leads to a more effective decoupling from the surface friction. For these conditions of strong atmospheric stratification and weak momentum transport by the LLJ, the cool air remains locally over the vegetated rural surfaces where it was generated through efficient radiative cooling during the cloud-free nights. Both advection and vertical mixing processes are weak and hence support the formation of very strong ΔUHI (Hu et al., 2013; Lin et al., 2022). Here we

demonstrate that σ_w^2, obtained commonly at one measurement location at a height above the roughness sublayer but below the LLJ core, can be considered a representative indicator of the vertical mixing in the nocturnal urban boundary layer and hence a powerful predictor for the UHI intensity.

Table 3. Mean values of core height (Z_{LLJ}), core wind speed (WS_{LLJ}) and the corresponding ΔUHI for each class of vertical velocity variance (σ_w^2).

σ_w^2 (m^{2}s^{-2})	< 0.11	$0.11 \leq \sigma_w^2 < 0.23$	≥ 0.23
WS_{LLJ} (ms^{-1})	6.2	8.0	10.1
Z_{LLJ} (m agl)	386	490	540
ΔUHI (°C)	5.39	3.05	1.80

Note that the relation between ΔUHI and σ_w^2 remains valid even during nights when no consistent LLJ was detected by the automatic procedure (black triangles in Fig 9b), and other synoptic processes (such as fronts) are likely to modulate the atmospheric mixing. 53% of the jet-free nights fall into the low σ_w^2 class (red shading), and all show ΔUHI > 3.5 °C. Future studies are going to investigate why there is no LLJ detected for some nights although a low σ_w^2 suggests a stable atmospheric stratification that is likely to favor decoupling.

4   Conclusions

This study presents the first comprehensive description of the characteristics of the summertime Low-Level Jet (LLJ) over the Paris region. LLJ events are detected automatically from continuous scanning Doppler Wind Lidar (DWL) measurements over the city centre, using a tailored algorithm amended from an existing method (Tuononen et al., 2017). A key feature of this study is the high temporal and spatial resolution of wind profile observations, which allow for LLJ variability to be captured in great detail. During the study period from June 15 to August 31, 2022, LLJs were identified on 55 nights (70% of the nights). Notably, observations at an urban and a suburban sites reveal the regional nature of the LLJ, with 90% of events detected at both sites. This study focuses on nights with cloud-free conditions; hence, six cloudy nights were excluded from the analysis, isolating 49 LLJ cases for detailed investigation.

As jets were rarely observed during the daytime, this work focuses on nocturnal jets between 18 and 09 UTC (20h and 11h local time). A comprehensive analysis of LLJ characteristics is presented here, including core height, wind speed, and wind direction. An exceptional predominant easterly and northeasterly flow during the summer of 2022 led to the detection of jets with mostly northeast flow origins (30°-60°), showing a mean core height of approximately $430 \, \text{m agl}$. Very few LLJs were detected under a southeast and east flow (190° and 300°). On average the core wind speed is $8.9 \, \text{m s}^{-1}$ and in an range between 4 and $12 \, \text{m s}^{-1}$.

To systematically assess the temporal variability of LLJ in the Paris region, both in terms of the nocturnal evolution and the night-to-night variability, we take a novel approach to classify LLJ events. Rather than grouping profiles according to the core wind speed, as is usually found in the literature, nocturnal events are defined with a certain continuity and then classified according to the magnitude of the vertical velocity variance (σ_w^2) below the jet core. Three LLJ classes (with weak, intermediate, and strong vertical mixing) were established based on the frequency distribution of σ_w^2. It was found that these mixing classes are a clear indicator for the core characteristics (speed, height, temporal evolution) of most LLJ events, and tend to depend on the wind direction of the synoptic flow. Jets with low σ_w^2 are predominantly observed with flow from the south to southeast ($105°$-$180°$), at low altitudes ($< 300\,\mathrm{m}$ agl) and with low to intermediate wind speeds ($< 6\,\mathrm{m\,s^{-1}}$). The intermediate σ_w^2 class is mainly found in the northwest sector ($300°$-$360°$), with intermediate core heights ($< 450\,\mathrm{m}$ agl) and core wind speeds ($< 8.3\,\mathrm{m\,s^{-1}}$). Jets in the strong mixing class are primarily found under northeasterly flow, with most cases detected in a narrow sector ($30°$-$60°$) at high altitudes $> 400\,\mathrm{m}$ agl and with strong wind speeds $> 8.5\,\mathrm{m\,s^{-1}}$.

The continuous DWL measurements and automatic detection provide novel insights into the nocturnal dynamics of the jets in the region. Most events persist from sunset to sunrise, with an average duration of $\approx 10\,\mathrm{h}$, showcasing oscillations in core wind speeds that peak around midnight. Additionally, a prevalent clockwise wind direction veering was observed in 57% of cases, with an average change in wind direction of $3.7\,^\circ\mathrm{h^{-1}}$. Notably, two outlier cases that fell into the intermediate σ_w^2 class exhibited a sharp eastward veering from the northwest, with low wind speeds and relatively low altitudes.

For LLJ events characterized by the distinct signature of oscillatory wind speed and core wind direction veering, the Inertial Oscillation (IO) formation mechanism is clearly evident. For others, changes in synoptic flow may cause variations in the geosptrophic wind that can mask this signature. The wind speed oscillation is found for most cases with strong σ_w^2 and medium to high wind speeds, while it hardly appears in weak LLJs with low σ_w^2. The wind direction veering occurs in all vertical mixing classes but is most pronounced in LLJs with strong σ_w^2. Four outliers with strong wind speeds and a late starting time in the low σ_w^2 class exhibit the oscillation signature. These cases, characterized by strong core wind speeds and low σ_w^2, are likely generated under very stable near-surface atmospheric stratification. Additionally, particularly low surface drag may favor the acceleration of these jets as they pass over a basin area of low topography east of Paris before reaching the urban site. Both the role of IO in LLJ formation over the Paris region and the impact of topography require further investigation.

In addition to the LLJ characterization, a key contribution of this work is the investigation of the impacts of the LLJ on the canopy layer Urban Heat Island (UHI) effect. The surface wind speed is a meaningful parameter that explains variations in UHI intensity, as they account for dynamic effects. Our results, however, reveal that σ_w^2 explains even more of the ΔUHI variability, as it also accounts for the mechanical mixing induced by the LLJ at the top of the nocturnal urban boundary layer. Using σ_w^2 as predictor results in a reduced Mean Absolute Error (MAE) of $0.63\,^\circ\mathrm{C}$ compared to the uncertainty when using surface wind speed to explain the ΔUHI variations (MAE = $1.23\,^\circ\mathrm{C}$). The LLJ core wind speed does not sufficiently characterise the advection and mixing processes that reduce ΔUHI intensity, as highlighted by four outlier events (16 and 19 July, and 11 and 13 August) with strong core wind speeds and weak σ_w^2 that are among the nights with the strongest UHI. Although the LLJ is not the only source of mechanical turbulence, this nocturnal phenomenon certainly plays a key role in UHI development.

This study demonstrates that the regional-scale synoptic flow in form of the LLJ has clear implications for conditions in the urban boundary layer down to the surface. The mechanical turbulence driven by the LLJ significantly affects spatial contrasts in air temperature between the city and its surroundings and likely also influences the dispersion of atmospheric pollutants. In the summer of 2022, the LLJ was a very frequent phenomenon with variable characteristics that often suggest inertial oscillation
550   plays a role in its formation. A better understanding of LLJ formation in response to synoptic pressure patterns and topography is required to fully grasp its interactions with the urban atmosphere.

Code and data availability.   The data sets will be available in the AERIS-PANAME database (https://paname.aeris-data.fr/) and the code will be available upon request.

Appendix A: UHI determination
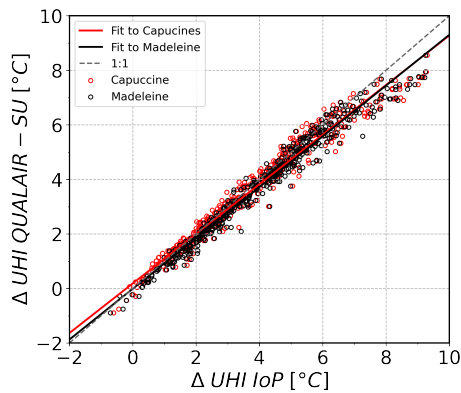
Figure A1. Comparison of ΔUHI = T_{urban} - T_{rural} calculated using a rooftop site at QUALAIR-SU (20 m agl) against ΔUHI determined for two street-level: Boulevard des Capucines and Place de la Madeleine. Solid lines represent the best linear fit for each group of data.

555   **Appendix B: LLJ impacts on UHI**

Author contributions.   JC, SK, LT, and MH worked on the conceptualization of this work. JC, MH, and JCD performed the WindCube scan 400s deployment and ensured continuous operation. JC, SK, LT, and MH designed the experiment and JC performed the measurements. AF performed the measurements and data curation of the WindCube scan WLS70. JC, SK, JP, and MAD worked on the computational algorithm implementation and data curation. JC, SK, JP, CT, LT, and MH conducted the investigation. JC writing of original draft. SK, CT, JP, LT, and
560   MH reviewed and edited the manuscript. MH, SK, and LT funding acquisition.
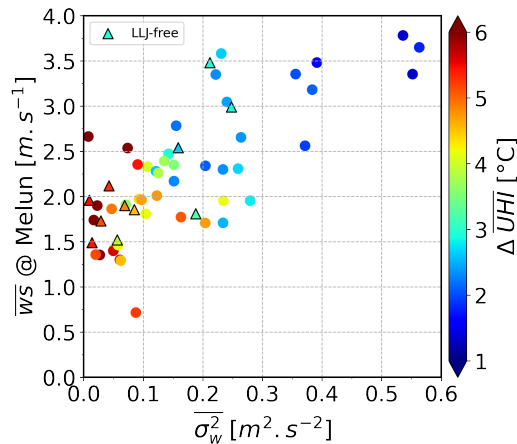
Figure B1. Nocturnal average of $10\,\mathrm{m}$ agl wind speed at Melun (rural site) as function of the nocturnal average vertical velocity variance (σ_w^2) at $238\,\mathrm{m}$ agl in the urban boundary layer, for all cloud-free nights in the study period. Data are colored by the the nocturnal average of $\Delta\mathrm{UHI}$. Dots represent nights with LLJ and the triangles the LLJ-free events.

Competing interests. The authors declare that they have no conflict of interest.

Acknowledgements. The authors thank OBS4CLIM ANR France 2030, DIM QI2 and ACTRIS-FR for financing the investment of the Doppler Wind Lidar (DWL) Vaisala WindCube Scan 400s. Jonnathan Céspedes is grateful to the Region île de France and VAISALA France SAS for funding the doctoral scholarship as part of the "Paris Region PhD 2020" program (Convention No 20007179). We thank the QUALAIR-SU platform for hosting the 400s and for the meteorological data, especially to Camille Viatte and Cristelle Cailteau-Fischbach. The authors are grateful to AERIS for providing SIRTA ReOBS data and support for PANAME (https://paname.aeris-data.fr/), as well as to Météo-France for the meteorological surface station data. Thanks to the SIRTA team, especially to Christophe Boitel for his technical support and to Jean-François Ribaud for support on the ReOBS data processing. The authors thank EDF R&D/CEREA for providing data collected by the DWL WLS70. This work is conducted in the context of the COST Action PROBE (CA18235), supported by COST (European Cooperation in Science and Technology, https://www.cost.eu/).

References

Algarra, I., Eiras-Barca, J., Nieto, R., and Gimeno, L.: Global climatology of nocturnal low-level jets and associated moisture sources and sinks, Atmospheric Research, 229, 39–59, https://doi.org/10.1016/J.ATMOSRES.2019.06.016, 2019.

Andreas, E. L., Claffey, K. J., and Makshtas, A. P.: Low-Level Atmospheric Jets And Inversions Over The Western Weddell Sea, Boundary-Layer Meteorology 2000 97:3, 97, 459–486, https://doi.org/10.1023/A:1002793831076, 2000.

Arfeuille, G., Quintanilla-Montoya, A. L., González, F. C. V., and Villarreal, L. Z.: Observational Characteristics of Low-Level Jets in Central Western Mexico, Boundary-Layer Meteorology, 155, 483–500, https://doi.org/10.1007/S10546-015-0005-0/METRICS, 2015.

Baas, P., Bosveld, F. C., Baltink, H. K., and Holtslag, A. A.: A Climatology of Nocturnal Low-Level Jets at Cabauw, Journal of Applied Meteorology and Climatology, 48, 1627–1642, https://doi.org/10.1175/2009JAMC1965.1, 2009.

Banta, R. M., Newsom, R. K., Lundquist, J. K., Pichugina, Y. L., Coulter, R. L., and Mahrt, L.: Nocturnal low-level jet characteristics over Kansas during cases-99, Boundary-Layer Meteorology, 105, 221–252, https://doi.org/10.1023/A:1019992330866/METRICS, 2002.

Banta, R. M., Pichugina, Y. L., and Newsom, R. K.: Relationship between Low-Level Jet Properties and Turbulence Kinetic Energy in the Nocturnal Stable Boundary Layer, Journal of the Atmospheric Sciences, 60, 2549 – 2555, https://doi.org/https://doi.org/10.1175/1520-0469(2003)060<2549:RBLJPA>2.0.CO;2, 2003.

Banta, R. M., Pichugina, Y. L., and Brewer, W. A.: Turbulent Velocity-Variance Profiles in the Stable Boundary Layer Generated by a Nocturnal Low-Level Jet, Journal of the Atmospheric Sciences, 63, 2700–2719, https://doi.org/10.1175/JAS3776.1, 2006.

Barlow, J. F., Halios, C. H., Lane, S. E., and Wood, C. R.: Observations of urban boundary layer structure during a strong urban heat island event, Environmental Fluid Mechanics 2014 15:2, 15, 373–398, https://doi.org/10.1007/S10652-014-9335-6, 2014.

Blackadar, A. K.: Boundary Layer Wind Maxima and Their Significance for the Growth of Nocturnal Inversions, Bulletin of the American Meteorological Society, 38, 283–290, https://doi.org/10.1175/1520-0477-38.5.283, 1957.

Bonin, T. A., Blumberg, W. G., Klein, P. M., and Chilson, P. B.: Thermodynamic and Turbulence Characteristics of the Southern Great Plains Nocturnal Boundary Layer Under Differing Turbulent Regimes, Boundary-Layer Meteorology, 157, 401–420, https://doi.org/10.1007/S10546-015-0072-2/METRICS, 2015.

Bonner, W. D.: Climatology of the Low Level Jet, Monthly Weather Review, 96, 833 – 850, https://doi.org/https://doi.org/10.1175/1520-0493(1968)096<0833:COTLLJ>2.0.CO;2, 1968.

Cariou, J. P., Boquet, M., Lolli, S., Parmentier, R., and Sauvage, L.: Validation of the new long range 1.5μm wind lidar WLS70 for atmospheric dynamics studies, https://doi.org/10.1117/12.830292, 7479, 180–189, https://doi.org/10.1117/12.830292, 2009.

Carroll, B. J., Demoz, B. B., and Delgado, R.: An Overview of Low-Level Jet Winds and Corresponding Mixed Layer Depths During PECAN, Journal of Geophysical Research: Atmospheres, 124, 9141–9160, https://doi.org/10.1029/2019JD030658, 2019.

Cheliotis, I., Dieudonné, E., Delbarre, H., Sokolov, A., Dmitriev, E., Augustin, P., Fourmentin, M., Ravetta, F., and Pelon, J.: Properties of Coherent Structures over Paris: A Study Based on an Automated Classification Method for Doppler Lidar Observations, Journal of Applied Meteorology and Climatology, 60, 1545–1559, https://doi.org/10.1175/JAMC-D-21-0014.1, 2021.

Chen, Y.-L., Tu, C.-C., Hsiao, F., Chen, C.-S., Lin, P.-L., and Lin, P.-H.: An Overview of Low-Level Jets (LLJs) and Their Roles in Heavy Rainfall over the Taiwan Area during the Early Summer Rainy Season, Meteorology 2022, Vol. 1, Pages 64-112, 1, 64–112, https://doi.org/10.3390/METEOROLOGY1010006, 2022.

Cheng, V., Ng, E., Chan, C., and Givoni, B.: Outdoor thermal comfort study in a sub-tropical climate: A longitudinal study based in Hong Kong, International Journal of Biometeorology, 56, 43–56, https://doi.org/10.1007/S00484-010-0396-Z/FIGURES/16, 2012.

Chiriaco, M., Dupont, J. C., Bastin, S., Badosa, J., Lopez, J., Haeffelin, M., Chepfer, H., and Guzman, R.: ReOBS: A new approach to synthesize long-term multi-variable dataset and application to the SIRTA supersite, Earth System Science Data, 10, 919–940, https://doi.org/10.5194/ESSD-10-919-2018, 2018.

Conangla, L. and Cuxart, J.: On the turbulence in the upper part of the low-level jet: An experimental and numerical study, Boundary-Layer Meteorology, 118, 379–400, https://doi.org/10.1007/S10546-005-0608-Y/METRICS, 2006.

Dieudonné, E., Delbarre, H., Sokolov, A., Ebojie, F., Augustin, P., and Fourmentin, M.: Characteristics of the low-level jets observed over Dunkerque (North Sea French coast) using 4 years of wind lidar data, Quarterly Journal of the Royal Meteorological Society, 149, 1745–1768, https://doi.org/10.1002/QJ.4480, 2023.

Dolfi-Bouteyre, A., Augère, B., Besson, C., Canat, G., Fleury, D., Gaudo, T., Goular, D., Lombard, L., Planchat, C., Valla, M., et al.: 1.5 μm all fiber pulsed lidar for wake vortex monitoring, in: Conference on Lasers and Electro-Optics, p. CMQ3, Optica Publishing Group, 2008.

Du, Y. and Chen, G.: Climatology of Low-Level Jets and Their Impact on Rainfall over Southern China during the Early-Summer Rainy Season, Journal of Climate, 32, 8813–8833, https://doi.org/10.1175/JCLI-D-19-0306.1, 2019.

Duarte, H. F., Leclerc, M. Y., Zhang, G., Durden, D., Kurzeja, R., Parker, M., and Werth, D.: Impact of Nocturnal Low-Level Jets on Near-Surface Turbulence Kinetic Energy, Boundary-Layer Meteorology, 156, 349–370, https://doi.org/10.1007/S10546-015-0030-Z/METRICS, 2015.

Dupont, J. C., Haeffelin, M., Badosa, J., Elias, T., Favez, O., Petit, J. E., Meleux, F., Sciare, J., Crenn, V., and Bonne, J. L.: Role of the boundary layer dynamics effects on an extreme air pollution event in Paris, Atmospheric Environment, 141, 571–579, https://doi.org/10.1016/J.ATMOSENV.2016.06.061, 2016.

ESA: Copernicus DEM - Global and European Digital Elevation Model (COP-DEM), https://doi.org/https://doi.org/10.5270/ESA-c5d3d65, 2023.

Gultepe, I., Sharman, R., Williams, P. D., Zhou, B., Ellrod, G., Minnis, P., Trier, S., Griffin, S., Yum, S. S., Gharabaghi, B., Feltz, W., Temimi, M., Pu, Z., Storer, L. N., Kneringer, P., Weston, M. J., ya Chuang, H., Thobois, L., Dimri, A. P., Dietz, S. J., França, G. B., Almeida, M. V., and Neto, F. L.: A Review of High Impact Weather for Aviation Meteorology, Pure and Applied Geophysics, 176, 1869–1921, https://doi.org/10.1007/S00024-019-02168-6/METRICS, 2019.

Haeffelin, M., Barthès, L., Bock, O., Boitel, C., Bony, S., Bouniol, D., Chepfer, H., Chiriaco, M., Cuesta, J., Delanoë, J., et al.: SIRTA, a ground-based atmospheric observatory for cloud and aerosol research, in: Annales Geophysicae, vol. 23, pp. 253–275, Copernicus, 2005.

Hartman, A. T.: An analysis of the effects of temperatures and circulations on the strength of the low-level jet in the Turkana Channel in East Africa, Theoretical and Applied Climatology, 132, 1003–1017, https://doi.org/10.1007/S00704-017-2121-X/METRICS, 2018.

He, Y., Yuan, C., Ren, C., Wang, W., Shi, Y., and Ng, E.: Urban ventilation assessment with improved vertical wind profile in high-density cities – Investigations in nighttime extreme heat, Building and Environment, 216, 109 018, https://doi.org/10.1016/J.BUILDENV.2022.109018, 2022.

Holton, J. R.: The diurnal boundary layer wind oscillation above sloping terrain, http://dx.doi.org/10.3402/tellusa.v19i2.9766, 19, 200–205, https://doi.org/10.3402/TELLUSA.V19I2.9766, 1967.

Hu, X. M., Klein, P. M., Xue, M., Lundquist, J. K., Zhang, F., and Qi, Y.: Impact of Low-Level Jets on the Nocturnal Urban Heat Island Intensity in Oklahoma City, Journal of Applied Meteorology and Climatology, 52, 1779–1802, https://doi.org/10.1175/JAMC-D-12-0256.1, 2013.

Jiménez-Sánchez, G., Markowski, P. M., Jewtoukoff, V., Young, G. S., and Stensrud, D. J.: The Orinoco Low-Level Jet: An Investigation of Its Characteristics and Evolution Using the WRF Model, Journal of Geophysical Research: Atmospheres, 124, 10 696–10 711, https://doi.org/10.1029/2019JD030934, 2019.

Kallistratova, M. A. and Kouznetsov, R. D.: Low-Level Jets in the Moscow Region in Summer and Winter Observed with a Sodar Network, Boundary-Layer Meteorology, 143, 159–175, https://doi.org/10.1007/S10546-011-9639-8/METRICS, 2012.

Kallistratova, M. A., Kouznetsov, R. D., Kramar, V. F., and Kuznetsov, D. D.: Profiles of Wind Speed Variances within Nocturnal Low-Level Jets Observed with a Sodar, Journal of Atmospheric and Oceanic Technology, 30, 1970–1977, https://doi.org/10.1175/JTECH-D-12-00265.1, 2013.

Karipot, A., Leclerc, M. Y., and Zhang, G.: Characteristics of Nocturnal Low-Level Jets Observed in the North Florida Area, Monthly Weather Review, 137, 2605–2621, https://doi.org/10.1175/2009MWR2705.1, 2009.

Klein, A., Ravetta, F., Thomas, J. L., Ancellet, G., Augustin, P., Wilson, R., Dieudonné, E., Fourmentin, M., Delbarre, H., and Pelon, J.: Influence of vertical mixing and nighttime transport on surface ozone variability in the morning in Paris and the surrounding region, Atmospheric Environment, 197, 92–102, https://doi.org/10.1016/J.ATMOSENV.2018.10.009, 2019.

Kong, F., Yan, W., Zheng, G., Yin, H., Cavan, G., Zhan, W., Zhang, N., and Cheng, L.: Retrieval of three-dimensional tree canopy and shade using terrestrial laser scanning (TLS) data to analyze the cooling effect of vegetation, Agricultural and Forest Meteorology, 217, 22–34, https://doi.org/10.1016/J.AGRFORMET.2015.11.005, 2016.

Kotthaus, S. and Grimmond, C. S. B.: Atmospheric boundary-layer characteristics from ceilometer measurements. Part 1: A new method to track mixed layer height and classify clouds, Quarterly Journal of the Royal Meteorological Society, 144, 1525–1538, https://doi.org/10.1002/QJ.3299, 2018.

Kotthaus, S., Haeffelin, M., Céspedes, J., Hove, M. V., Drouin, M.-A., Dupont, J.-C., and Foret, G.: Urban atmosphere dynamics for air quality applications: Atmospheric boundary layer height and wind profiles from ground-based remote sensing networks, EGU23, https://doi.org/10.5194/EGUSPHERE-EGU23-13154, 2023.

Lemonsu, A. and Masson, V.: Simulation of a Summer Urban Breeze Over Paris, Boundary-Layer Meteorology 2002 104:3, 104, 463–490, https://doi.org/10.1023/A:1016509614936, 2002.

Li, X. and Du, Y.: Statistical Relationships between Two Types of Heavy Rainfall and Low-Level Jets in South China, Journal of Climate, 34, 8549–8566, https://doi.org/10.1175/JCLI-D-21-0121.1, 2021.

Li, X., Zhang, C., Li, W., Anyah, R. O., and Tian, J.: Exploring the trend, prediction and driving forces of aerosols using satellite and ground data, and implications for climate change mitigation, Journal of Cleaner Production, 223, 238–251, https://doi.org/10.1016/J.JCLEPRO.2019.03.121, 2019.

Lin, Y., Wang, C., Yan, J., Li, J., and He, S.: Observation and Simulation of Low-Level Jet Impacts on 3D Urban Heat Islands in Beijing: A Case Study, Journal of the Atmospheric Sciences, 79, 2059–2073, https://doi.org/10.1175/JAS-D-21-0245.1, 2022.

Liu, H., He, M., Wang, B., and Zhang, Q.: Advances in low-level jet research and future prospects, Journal of Meteorological Research, 28, 57–75, https://doi.org/10.1007/S13351-014-3166-8/METRICS, 2014.

Liu, Z., Barlow, J. F., Chan, P. W., Fung, J. C. H., Li, Y., Ren, C., Mak, H. W. L., and Ng, E.: A Review of Progress and Applications of Pulsed Doppler Wind LiDARs, Remote Sensing 2019, Vol. 11, Page 2522, 11, 2522, https://doi.org/10.3390/RS11212522, 2019.

Luiz, E. W. and Fiedler, S.: Spatiotemporal observations of nocturnal low-level jets and impacts on wind power production, Wind Energy Science, 7, 1575–1591, https://doi.org/10.5194/WES-7-1575-2022, 2022.

Lundquist, J. K.: Wind Shear and Wind Veer Effects on Wind Turbines, Handbook of Wind Energy Aerodynamics, pp. 1–22, https://doi.org/10.1007/978-3-030-05455-7_44-1, 2021.

Marke, T., Crewell, S., Schemann, V., Schween, J. H., and Tuononen, M.: Long-Term Observations and High-Resolution Modeling of Midlatitude Nocturnal Boundary Layer Processes Connected to Low-Level Jets, Journal of Applied Meteorology and Climatology, 57, 1155–1170, https://doi.org/10.1175/JAMC-D-17-0341.1, 2018.

Oke, T. R.: City size and the urban heat island, Atmospheric Environment (1967), 7, 769–779, https://doi.org/10.1016/0004-6981(73)90140-6, 1973.

Oke, T. R., Mills, G., Christen, A., and Voogt, J. A.: Urban Heat Island, p. 197–237, Cambridge University Press, https://doi.org/10.1017/9781139016476.008, 2017.

Pal, S., Xueref-Remy, I., Ammoura, L., Chazette, P., Gibert, F., Royer, P., Dieudonné, E., Dupont, J. C., Haeffelin, M., Lac, C., Lopez, M., Morille, Y., and Ravetta, F.: Spatio-temporal variability of the atmospheric boundary layer depth over the Paris agglomeration: An assessment of the impact of the urban heat island intensity, Atmospheric Environment, 63, 261–275, https://doi.org/10.1016/J.ATMOSENV.2012.09.046, 2012.

Pearson, G., Davies, F., and Collier, C.: An Analysis of the Performance of the UFAM Pulsed Doppler Lidar for Observing the Boundary Layer, Journal of Atmospheric and Oceanic Technology, 26, 240–250, https://doi.org/10.1175/2008JTECHA1128.1, 2009.

Petit, J.-E., Gros, V., Favez, O., Simon, L., Kalalian, C., Brugère, E., Borbon, A., Dupont, J.-C., Abbou, G., Ghersi, V., et al.: Forest fire plumes in the Paris region (France) during summer 2022, the spoor of a schorching summer, Tech. rep., Copernicus Meetings, 2023.

Qi, L., Leslie, L. M., and Zhao, S. X.: Cut-off low pressure systems over southern australia: climatology and case study, INTERNATIONAL JOURNAL OF CLIMATOLOGY Int. J. Climatol, 19, 1633–1649, https://doi.org/10.1002/(SICI)1097-0088(199912)19:15, 1999.

Qualair: Site Qualair, http://qualair.aero.jussieu.fr/qualair.php?menu=present, accessed: 2022-06-11, 2022.

Region, L. P.: Ilots de chaleur Urbains (ICU) : classification des IMU en zone climatique locale (LCZ) , Aléas et Vulnérabilités à la chaleur de Jour et de Nuit en Île-de-France, https://data-iau-idf.opendata.arcgis.com/datasets/iau-idf::ilots-de-chaleur-urbains-icu-classification-des-imu-en-zone-climatique-locale-lcz-al%C3%A9as-et-vuln%C3%A9rabilit%C3%A9s-%C3%A0-la-chaleur-de-jour-et-de-nuit-en-%C3%AEle-de-france/about, 2023.

Ridder, K. D., Maiheu, B., Lauwaet, D., Daglis, I. A., Keramitsoglou, I., Kourtidis, K., Manunta, P., and Paganini, M.: Urban Heat Island Intensification during Hot Spells—The Case of Paris during the Summer of 2003, Urban Science 2017, Vol. 1, Page 3, 1, 3, https://doi.org/10.3390/URBANSCI1010003, 2016.

Robine, J. M., Cheung, S. L. K., Roy, S. L., Oyen, H. V., Griffiths, C., Michel, J. P., and Herrmann, F. R.: Death toll exceeded 70,000 in Europe during the summer of 2003, Comptes Rendus Biologies, 331, 171–178, https://doi.org/10.1016/J.CRVI.2007.12.001, 2008.

Roy, S., Sentchev, A., Schmitt, F. G., Augustin, P., and Fourmentin, M.: Impact of the Nocturnal Low-Level Jet and Orographic Waves on Turbulent Motions and Energy Fluxes in the Lower Atmospheric Boundary Layer, Boundary-Layer Meteorology 2021 180:3, 180, 527–542, https://doi.org/10.1007/S10546-021-00629-X, 2021.

Roy, S., Sentchev, A., Fourmentin, M., and Augustin, P.: Machine Learning and Deterministic Methods for Detection Meteorological Phenomena from Ground Measurements: Application for Low-Level Jet and Sea-Breeze Identification in Northern France, Atmosphere 2022, Vol. 13, Page 1873, 13, 1873, https://doi.org/10.3390/ATMOS13111873, 2022.

Rubio, H., Kühn, M., and Gottschall, J.: Evaluation of low-level jets in the southern Baltic Sea: a comparison between ship-based lidar observational data and numerical models, Wind Energy Science, 7, 2433–2455, https://doi.org/10.5194/WES-7-2433-2022, 2022.

Shapiro, A., Fedorovich, E., and Rahimi, S.: A Unified Theory for the Great Plains Nocturnal Low-Level Jet, Journal of the Atmospheric Sciences, 73, 3037–3057, https://doi.org/10.1175/JAS-D-15-0307.1, 2016.

720 Stull, R. B.: Stable Boundary Layer, An Introduction to Boundary Layer Meteorology, pp. 499–543, https://doi.org/10.1007/978-94-009-3027-8_12, 1988.

Sánchez, M. P., de Oliveira, A. P., Varona, R. P., Tito, J. V., Codato, G., Ribeiro, F. N. D., Filho, E. P. M., and da Silveira, L. C.: Rawinsonde-Based Analysis of the Urban Boundary Layer in the Metropolitan Region of São Paulo, Brazil, Earth and Space Science, 7, e2019EA000 781, https://doi.org/10.1029/2019EA000781, 2020.

725 Sánchez, M. P., Pereira de Oliveira, A., Varona, R. P., Tito, J. V., Codato, G., Ynoue, R. Y., Ribeiro, F. N. D., Marques Filho, E. P., and da Silveira, L. C.: Observational Investigation of the Low-Level Jets in the Metropolitan Region of São Paulo, Brazil, Earth and Space Science, 9, e2021EA002 190, https://doi.org/https://doi.org/10.1029/2021EA002190, 2022.

Taylor, J., Wilkinson, P., Davies, M., Armstrong, B., Chalabi, Z., Mavrogianni, A., Symonds, P., Oikonomou, E., and Bohnenstengel, S. I.: Mapping the effects of urban heat island, housing, and age on excess heat-related mortality in London, Urban Climate, 14, 517–528,
730 https://doi.org/10.1016/J.UCLIM.2015.08.001, 2015.

Theeuwes, N. E., Barlow, J. F., Teuling, A. J., Grimmond, C. S. B., and Kotthaus, S.: Persistent cloud cover over mega-cities linked to surface heat release, npj Climate and Atmospheric Science 2019 2:1, 2, 1–6, https://doi.org/10.1038/s41612-019-0072-x, 2019.

Thobois, L., Cariou, J. P., and Gultepe, I.: Review of Lidar-Based Applications for Aviation Weather, Pure and Applied Geophysics, 176, 1959–1976, https://doi.org/10.1007/S00024-018-2058-8/FIGURES/12, 2019.

735 Tsiringakis, A., Theeuwes, N. E., Barlow, J. F., and Steeneveld, G. J.: Interactions Between the Nocturnal Low-Level Jets and the Urban Boundary Layer: A Case Study over London, Boundary-Layer Meteorology, 183, 249–272, https://doi.org/10.1007/S10546-021-00681-7/FIGURES/9, 2022.

Tuononen, M., Sinclair, V. A., and Vihma, T.: A climatology of low-level jets in the mid-latitudes and polar regions of the Northern Hemisphere, Atmospheric Science Letters, 16, 492–499, https://doi.org/10.1002/ASL.587, 2015.

740 Tuononen, M., O'Connor, E. J., Sinclair, V. A., and Vakkari, V.: Low-Level Jets over Utö, Finland, Based on Doppler Lidar Observations, Journal of Applied Meteorology and Climatology, 56, 2577–2594, https://doi.org/10.1175/JAMC-D-16-0411.1, 2017.

Ulpiani, G.: On the linkage between urban heat island and urban pollution island: Three-decade literature review towards a conceptual framework, Science of The Total Environment, 751, 141 727, https://doi.org/10.1016/J.SCITOTENV.2020.141727, 2021.

van de Wiel, B. J., Moene, A. F., Steeneveld, G. J., Baas, P., Bosveld, F. C., and Holtslag, A. A.: A Conceptual View on Inertial Oscillations
745 and Nocturnal Low-Level Jets, Journal of the Atmospheric Sciences, 67, 2679–2689, https://doi.org/10.1175/2010JAS3289.1, 2010.

Vanderwende, B. J., Lundquist, J. K., Rhodes, M. E., Takle, E. S., and Irvin, S. L.: Observing and Simulating the Summertime Low-Level Jet in Central Iowa, Monthly Weather Review, 143, 2319–2336, https://doi.org/10.1175/MWR-D-14-00325.1, 2015.

Wei, W., Wu, B. G., Ye, X. X., Wang, H. X., and Zhang, H. S.: Characteristics and Mechanisms of Low-Level Jets in the Yangtze River Delta of China, Boundary-Layer Meteorology, 149, 403–424, https://doi.org/10.1007/S10546-013-9852-8/FIGURES/13, 2013.

750 Wei, W., Zhang, H., Zhang, X., and Che, H.: Low-level jets and their implications on air pollution: A review, Frontiers in Environmental Science, 10, 1082 623, https://doi.org/10.3389/FENVS.2022.1082623/BIBTEX, 2023.

Whiteman, C. D., Bian, X., and Zhong, S.: Low-Level Jet Climatology from Enhanced Rawinsonde Observations at a Site in the Southern Great Plains, Journal of Applied Meteorology, 36, 1363 – 1376, https://doi.org/https://doi.org/10.1175/1520-0450(1997)036<1363:LLJCFE>2.0.CO;2, 1997.

755 Wouters, H., Ridder, K. D., Demuzere, M., Lauwaet, D., and Lipzig, N. P. V.: The diurnal evolution of the urban heat island of Paris: A model-based case study during Summer 2006, Atmospheric Chemistry and Physics, 13, 8525–8541, https://doi.org/10.5194/ACP-13-8525-2013, 2013.